FINAL REPORT

Military Tactical Aircraft Engine Noise Matching to Infrared Signatures

SERDP Project WP-2404

JANUARY 2016

Dr. Phillip Cunio
Reed A. Weber
Kimberly R. Knobel
Christine Smith
Air Force Research Laboratory

Andy Draudt
Aerodyne Research, Inc.

SERDP
DOD ▪ EPA ▪ DOE

REPORT DOCUMENTATION PAGE

Form Approved
OMB No. 0704-0188

1. REPORT DATE *(DD-MM-YYYY)*	2. REPORT TYPE	3. DATES COVERED *(From - To)*
16/12/2016	Final Report	04/01/2016 - 12/01/2016

4. TITLE AND SUBTITLE

Military Tactical Aircraft Engine Noise Matching to Infrared Signatures

5a. CONTRACT NUMBER

5b. GRANT NUMBER

5c. PROGRAM ELEMENT NUMBER

6. AUTHOR(S)
Phillip Cunio, Reed A. Weber, Kimberly R. Knobel, Christine Smith
Air Force Research Laboratory

Andy Draudt
Aerodyne Research, Inc.

5d. PROJECT NUMBER
WP-2404

5e. TASK NUMBER

5f. WORK UNIT NUMBER

7. PERFORMING ORGANIZATION NAME(S) AND ADDRESS(ES)
Air Force Research Laboratory/Space Vehicles
3550 Aberdeen Ave SE
Kirtland AFB, NM 87117

8. PERFORMING ORGANIZATION REPORT NUMBER

9. SPONSORING/MONITORING AGENCY NAME(S) AND ADDRESS(ES)
Strategic Environmental Research and Development Program
4800 Mark Center Drive
Suite 17D03
Alexandria, VA 22350-3605

10. SPONSOR/MONITOR'S ACRONYM(S)
ESTCP

11. SPONSOR/MONITOR'S REPORT NUMBER(S)

12. DISTRIBUTION/AVAILABILITY STATEMENT
Approved for public release; distribution is unlimited.

13. SUPPLEMENTARY NOTES
N/A

14. ABSTRACT

This report builds on theoretical analysis of jet engine infrared signatures and their potential relationships to jet engine acoustic emissions in order to identify the region of a jet engine plume most likely to emit both in temporal infrared and in acoustic domains. As a means of verifying initial assessments that infrared and acoustic emissions are connected via physics-based mechanisms, a field campaign to collect relevant data was carried out with a bank of infrared instruments imaging a T700 turboshaft engine undergoing routine operational testing, while microphones collected simultaneous acoustic data.

15. SUBJECT TERMS
Aircraft engine noise, jet engine infrared signatures, hypertemporal imaging, acoustic emissions.

16. SECURITY CLASSIFICATION OF:			17. LIMITATION OF ABSTRACT	18. NUMBER OF PAGES	19a. NAME OF RESPONSIBLE PERSON
a. REPORT	b. ABSTRACT	c. THIS PAGE			Phillip Cunio
Unclassified	Unclassified	UU	UL	41	19b. TELEPHONE NUMBER *(Include area code)* 505-853-7822

Page Intentionally Left Blank

Page Intentionally Left Blank

FRONT MATTER

TABLE OF CONTENTS

LIST OF FIGURES

LIST OF ACRONYMS

AC – Alternating Current
AFB – Air Force Base
CFD – Computational Fluid Dynamics
CO2 – Carbon Dioxide
FY – Fiscal Year
IR – Infrared
KAFB – Kirtland Air Force Base
LES – Large Eddy Simulation
LWIR – Long-Wave Infrared
MWIR – Mid-Wave Infrared
OSD – Office of the Secretary of Defense
PC – Principal Component
PCA – Principal Component Analysis
PSD – Power Spectral Density
RMS – Root Mean Square
RPM – Repetitions per Minute
SPL – Sound Pressure Level
SWIR – Short-Wave Infrared

KEYWORDS

fast framing, jet engine plume, acoustic noise, electro-optical imaging, flight line environment, infrared signatures, acoustic signatures

ACKNOWLEDGMENTS

The authors of this report acknowledge and thank the Office of the Secretary of Defense (OSD) for the funding provided in support of this work.

ABSTRACT

Objectives

This report builds on theoretical analysis of jet engine infrared signatures and their potential relationships to jet engine acoustic emissions in order to identify the region of a jet engine plume most likely to emit both in temporal infrared and in acoustic domains. As a means of verifying initial assessments that infrared and acoustic emissions are connected via physics-based mechanisms, a field campaign to collect relevant data was carried out with a bank of infrared instruments imaging a T700 turboshaft engine undergoing routine operational testing, while microphones collected simultaneous acoustic data. In-depth mathematical analyses using principal component analysis and power spectral density analyses were conducted on the infrared and acoustic data to determine whether any relationship exists between infrared emissions and acoustic emissions.

Technical Approach

Hypertemporal imaging uses fast-framed image data (typically hundreds or thousands of frames per second), together with time-domain analysis, to extract dim fluctuating signals, especially against bright backgrounds. Principal component analysis is commonly used as a means of dimensional reduction, transforming observations into correlated subsets called principal components, which are linearly uncorrelated to each other. Here PCA can reveal spatial patterns of temporal correlation.

To collect data for this effort, a mid-wave infrared (MWIR) camera (model FLIR SC6701, bandwidth 3-5 μm, with a 50 mm f/2.5 lens) was set to stare at a jet engine plume, about 5-6 jet diameters away from the exhaust plane. Acoustic sensors were also emplaced around the plume, including on a line directly between the instruments and the expected maximum-emissions zone. The engine was run at a careful throttle profile, and the MWIR camera collected data (10 seconds @ 120 Hz – max capture rate) at each throttle setting. Throttle settings were held for 10-30 seconds, and then a ramp up or down to a new setting was completed. A given engine run would incorporate from two to four different throttle settings, and would last approximately ten minutes. Altogether, three engine runs were completed, and data was captured from at least one throttle setting.

Data were analyzed via three methods. To determine spatial regions of temporal correlation, principal components analysis was performed on the frames of the infrared imagery data in order to separate sources of IR fluctuations. This produced a single image showing the RMS AC signal of each pixel time history. These images illustrated plume structure and the fluctuating regions of IR energy transfer in the plume. Comparing figures reveals that plume structures change in size as throttle levels rise; additional features make it clear highly complex fluid flow is being observed.

To determine differences in temporal PSD signature, a PSD of the time history of the maximum pixel in each specific principal component was generated to show the power spectral density. This was to search for a spike in the PSD at a frequency known to be the same as, or perhaps a harmonic of, an acoustic frequency with strong emissions – no such obvious spikes were uncovered, although further analysis, including: 1) calculations of the correlation with acoustic data (cf. Section 5.4); 2) interrogation of the spectral phase indicated by each principal component; 3) reliance upon higher frame rate MWIR imagers would be desirable.

To perform acoustic analysis, pressure spectra (sound pressure levels across frequencies, with a total SPL listed at the top) on the left, and spectrograms (sound levels over a thin slice of time during that zone era, at various frequencies, with darker red indicating more power) were used. Spikes appear at below 200 Hz, about 350 Hz, transiently near 650 Hz, and very broadly at just over 1000 Hz.

In general, there is some apparent structure in the acoustic noise, and there is also evidence of features of this structure changing as the throttle settings change. While all this is to be expected, any correlation detected between this and the hypertemporal structure detected in the plume may show how the two are related. Unfortunately, all of the most prominent acoustic features lie outside the range accessible by the imagers employed, although some correlations were observable.

The spike data is then used to determine the correlation relationship between IR and Acoustic data and plot it spatially. Low-pass filtered acoustic data, extracted to match timing of infrared imagery data, is covariance-mapped in its time history to the time history of the infrared imagery data.

Results

Analysis of simultaneously acquired acoustic and IR measurements of a T700 engine under test yielded several notable conclusions relevant to using hypertemporal imaging techniques to aid in mitigating jet engine noise generation.

An analysis of MWIR data alone indicates the specific structure of correlated energy transfer processes within the engine plume down to significantly small spatial scales and at significantly small AC contributions. Such fine resolution may be very useful by itself as truth data for refining computational fluid dynamics models used when designing jet engines. Such additional refinement may lead to greater success in mitigating jet engine noise via design.

Direct analysis of the acoustic data indicated that the most prominent noise features are present at frequencies beyond the frame rate capabilities of the IR imagers used in this analysis. However, IR imagers with adequate frame rates (>500 Hz) may be acquired for future work based on this effort.

Of most significance here, the analysis incorporating both MWIR and acoustic data indicates regions of high correlation with clear structure. In this way, at least some of the dynamics of the engine plume that are responsible for acoustic generation are clearly captured by IR observations. Viewed in light of the principal components images of Section 5.1, striking similarities make it appear that the regions of highest correlation coincide with the energy transfer processes captured by principal components between 5 and 25. If these processes can be understood and separated from non-noise generating flow, mitigation of such processes could be prioritized when designing quiet jet engines.

Benefits

Jet engine noise can be both a health hazard and an environmental pollutant, particularly affecting personnel working in close proximity to jet engines, such as airline baggage handlers and mechanics. Mitigating exposure to jet engine noise could reduce the potential for hearing loss in runway workers; however, there exists a very complex relationship between jet engine design parameters, operating conditions, and resultant noise power levels. We demonstrate initial results highlighting the utility of high-speed imaging (also called hypertemporal imaging) in correlating the infrared signatures of jet aircraft engines with acoustic noise from the jet engines. This detection enables the use of a new domain in characterizing jet engine noise, which may in turn enable new methods of predicting or mitigating jet engine noise, which could lead to socioeconomic benefits for airlines and other operators of large numbers of jet engines.

BODY

1. OBJECTIVE

It is desirable to better predict jet engine acoustic noise characteristics in order to avoid negative health effects on people who work near jet engines on a regular basis. As part of this, it is desirable to understand jet engine noise emission based on design characteristics. This type of noise prediction proves to be a difficult problem, since the inherent complexity of turbulent fluctuations in a jet flow has yet to be well described by a generalized theory. While large eddy simulation (LES) is used with some success in predicting acoustic noise generation[1], it is thus far lacking in the resolution required to fully examine and validate the effects of small-scale turbulent flow which may dominate sound generation under certain engine operating conditions.

This report describes theoretical analysis and a field campaign using hypertemporal imaging to correlate jet engine noise and small-scale turbulent flow characteristics. Such small-scale flow characteristics are believed to be the dominant source of noise generation in subsonic jets[2] and may be predictable during design phases if experimental techniques are developed to adequately inform and validate the fine resolution behavior of fluid dynamics models regularly used in engine design. Alternatively, it may be possible to use image-processing techniques to observe jet plumes in the infrared and to detect, without the use of microphones physically located near the plumes, some characteristics of the plume which correlate in known ways to acoustic characteristics of the plume. If this can be accomplished, then it might be feasible to track the locations of plume regions emitting acoustic spectra known to be particularly damaging to human hearing, using only remotely-sited infrared sensors. This might help in organizing flight line operations in ways that could limit exposure to damaging acoustic spectra by flight line personnel.

The success criteria for this Limited Scope effort involve the collection of sufficient data to determine whether hypertemporal signatures are or are likely present in jet engine infrared emissions and whether there is any initial evidence of their being correlated to acoustic emissions. If a) hypertemporal characteristics can be detected in a jet engine plume's infrared emissions, and b) some evidence can be observed of a correlation, covariation, or other connection between these hypertemporal signatures and the jet engine plume's acoustic emissions, then this pilot project can be accounted successful.

These two criteria each buy down the risk of investing in a full-scale field campaign by indicating that a) the phenomenon that would be apparent to infrared sensors is both present and detectable, and that b) this phenomenon shows some change when acoustic emissions change. Meeting these criteria thus ensure that a follow-on full-scale field campaign can be assured of the existence of these connected phenomena, and can seek to quantify and characterize their relationship rather than simply to uncover it.

2. BACKGROUND

Hypertemporal imaging proved to be a useful technique either for understanding small-scale flow characteristics or for detecting and tracking plume regions associated with particular acoustic spectra, in that hypertemporal imaging is capable of detecting small correlated signals against complex backgrounds. The jet engine flow characteristics that correlate most closely to acoustic noise characteristics are dim signals, which present themselves as barely discernible patterns in the environment of a high-speed jet flow. These correlations, amenable to hypertemporal imaging characterization of jet engine plumes, may ultimately lead to an ability to predict and control jet engine acoustic noise, or to manage flight line operations for maximum long-term health benefits.

2.1 Acoustic noise and temporal variations

The basic measure of acoustic energy is sound pressure level, or SPL. SPL is defined as $20 \log P_{rms} / P_0$, where $P_0 = 2 \times 10^{-5}\ N/m^2$ is the commonly accepted threshold of human hearing at 1 kHz. Notably, with respect to jet engine flow dynamics, a sudden variation of temporal volumetric flow produces loud noise, whereas slowly varying flow features by themselves account for lesser SPL noise generation.[3] Thus it is sensible to attempt to detect and analyze the effects of even small temporal variations on overall noise.

The temporal variation in SPL (and noise frequency) from jet engines is also known to have some effect on human perception of the noise; for example, variations in takeoff noise exhibit amplitudes of 2-8 dB (at the fifth harmonic, which shows a very high temporal variation) at 4697 Hz.[4] This provides some additional justification for considering temporal variation in jet engine plumes as potentially related to temporal variation in overall acoustic noise.

2.2 Jet engine plume acoustic variations

In the design parameter space of jet engines, the nozzle geometry clearly influences sound generation and may be a key parameter in noise mitigation. Serrated nozzles (chevron nozzles) are known to produce improved mixing in the turbulent exhaust of an engine and have been observed to decrease noise.[5,10] In fact, studies on programmable nozzles have shown the ability to create significantly less engine noise due to the improved mixing that yields reduced coherent structure in the resultant flow field. One interpretation of this result involves wave packet formation as a significant corollary of acoustic generation, as described below.

However, most noise calculations used in aircraft noise studies focus on flying aircraft, rather than on aircraft on ramps or runways.[5] On takeoff, jet and fan noise dominate, while on landing the turbine, combustion chamber, compressor, nozzle and bleed valves all play a role.[5] This work focused on jet noise, as we are most interested in ramp activities and takeoff (since these are the situations where flight line workers, perhaps particularly military flight line workers, are most often near noise).[12]

Jet noise itself is a complex phenomenon, incorporating a variety of frequencies and tones. Even though lower-frequency components may initially seem the dominant component, this may be due to the fact that the greatest body of work done on jet engine noise focuses on noise produced by jet engines flying overhead, such that the lower-frequency noise is the perceptually dominant

component, due to the geometry of the event. However, other types of noise may be of equal interest for this work, including mixes of higher-frequency noise. Jet engine crackle (a mix of intermittent high and low pressure, lasting roughly 5 msec per event[15]) is regarded as one of the more salient features of jet engine acoustic emissions, and does not seem to incorporate substantially lower frequencies. Small-scale turbulence also becomes the dominant noise source under some conditions, including low Mach number jets, and radiates in all directions[16].

Additionally, in a flight-line environment, noise that propagates directly aft may be of less interest due to the fact that standing directly behind operating jet engines is generally not something flight line personnel do, whereas noise that propagates at some angle (cf. Figure 1 for a visualization of the maximum noise emission angle, which is not directly aft) can have a more important effect on personnel, even though it may not be the most dominant noise source.

2.3 Jet engine plume acoustic and thermal characteristics

Jet noise, or plume noise, is caused by the turbulent mixing of a free jet with ambient air. In general, turbulent structures grow as they get further from nozzle, creating a lowering of their frequencies. The maximum strength of the acoustic source (modeled as a chain of sources stretching away from the nozzle) occurs at the end of the potential core of the jet, about 5-6 jet diameters away from the nozzle exit. The directivity of this acoustic source varies, and reaches a maximum at 135-150 degrees away from the engine inlet.

Figure 1 shows how the aspect angles of maximum plume acoustic and infrared emissions align. It is noteworthy that the angle of maximum acoustic emissions corresponds to the angle where infrared emissions are dominated by the exhaust plume and the engine’s visible hot parts.

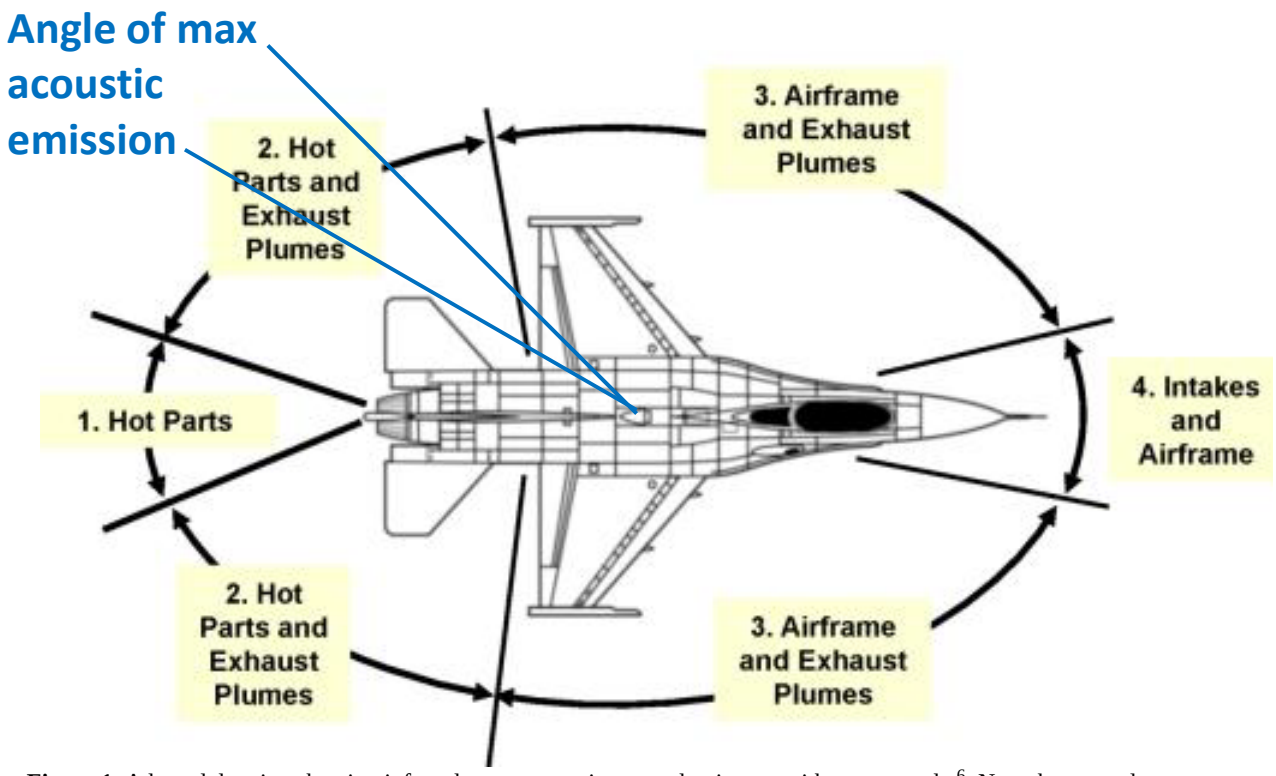

Figure 1. Adapted drawing showing infrared component signature dominance with aspect angle.[6] Note the general characteristic that exhaust plume noise maximum directivity corresponds to the exhaust plume infrared emission maximum directivity (in the after quarter aspect).

There is also some spatial variation present in jet engine acoustic characteristics. According to Bogey, Bailly, and Juve,[1] there is an origin point for predominant sound sources in the jet, located near the end of the potential core, at some number of jet diameters away from the exhaust nozzle. This suggests that the turbulent mixing and other flow dynamics present at this location may be of great interest for efforts intended to reduce noise emission, and therefore we have focused data collection efforts on approximately this location in the jet plume.

Jet engine exhaust plumes also exhibit emission and absorption of radiation from their emitted chemical species, occurring at discrete spectra. Two chemical species with emission/absorption lines in the MWIR region are CO2 and water vapor. These species are commonly present in exhaust plumes, as they are the primary combustion byproducts of hydrocarbon fuels. However, the Earth's atmosphere also contains water vapor and CO2, and demonstrates emission/absorption lines at the same wavelengths. As a result, plume emissions are absorbed by passage through the atmosphere to a greater degree than emissions from hot parts and the airframe. This leads to a focus on long-range detection in the IR regime via emissions from hot turbine parts or the airframe, often in the mid-wave IR or long-wave IR regimes.

We, however, have collected test data from a short range (5-10 m), thereby rendering insignificant the absorptive effects of atmosphere. Because the plume is the primary source of acoustic emissions in situations that are of concern to this work, we focused directly on the plume for infrared

emissions, rather than the secondary acoustic and thermal effects most likely associated with the airframe. This was accomplished by observing an isolated engine on a test stand.

2.4 Temporal and acoustic structure in jet engine plumes

Ogg[7] has examined remote sensing of temporal modulation of exhaust plume radiance. By modeling the turbofan acoustic signature, Ogg confirmed dependency between acoustic energy produced and fluctuations of the plume radiance. Furthermore, Ogg found that the temperature power spectral density had a peak value at around 400 Hz. When compared to the acoustic measurements made simultaneously, a peak in the core noise occurred at the same frequency. This is presented as strong evidence of a connection between the two phenomena.

Additionally, according to Sinha et al.,[8] the greatest noise is produced by the exhaust plume, confirming that this is an area that needs to be studied if we want to mitigate noise pollution from jet aircraft. According to Bogey et. al. [1] and Jordan and Colonius,[9] the degree of noise is determined by the interaction of wave packets, which is partly informed by the Reynolds number.

Wave packets manifest as coherent structures in jet plumes. These structures are moving local areas of different flow characteristics, including pressure or Mach waves, and may be visualized as something like a “train of puffs.” These “puffs” slowly evolve as they move down the plume, and are different from turbulence in that they exhibit significant coherence as they propagate.[9] Jordan and Colonius suggest that wave-packet analysis “may enable noise-reduction mechanisms to be developed and explained in a self-consistent manner.” [9]

Small-scale features hidden by a bright background, such as these wave packet interactions, can often be extracted by hypertemporal techniques, which can detect variations of small magnitude and short duration compared to the overall characteristics of the plume.

2.5 Hypertemporal imaging

Hypertemporal imaging uses fast-framed image data (typically hundreds or thousands of frames per second), together with time-domain analysis, to extract dim fluctuating signals, especially against bright backgrounds. Stacking a series of fast-framed images together along the time axis, the technique known as principal component analysis (PCA) can be used to determine which minor signal fluctuations are noise, and which display time-axis behavior characteristic of particular events occurring. Principal component analysis is commonly used as a means of dimensional reduction, transforming video observations into correlated subsets of the data, called principal components, which are linearly uncorrelated (orthogonal) to each other. In this report, PCA was used to reveal spatial patterns of temporal correlations.

The goal of this experiment was to detect, if present, distinct hypertemporal signatures and match them, if possible, to acoustic characteristics of the plume. In general, it may be that a particular hypertemporal signature is present, and increases in strength simultaneously with increases in jet engine acoustic noise. It may be that various hypertemporal signatures appear and fade as the noise level grows. In any case, if a characteristic hypertemporal signature is present, it may be correlatable to plume phenomena, such as wave packet generation or interaction, which would then connect acoustic jet engine noise to plume physics, meaning that a path forward can be laid between

engine design techniques and resultant noise properties, giving a whole new angle on understanding jet engine acoustic noise.

It should be noted that in the results that follow, the most success was achieved using a MWIR camera with maximum frame rate of 120 Hz. Thus, the correlations with acoustic data were limited to frequencies below 60 Hz. Fortunately, HTI analysis techniques do yield meaningful results even when the phenomena of interest is not greatly oversampled. Furthermore, at 120 Hz framerate the field of view does allow for tracking of bulk fluid dynamic flow, which occurs at speeds significantly below the speed of sound in low thrust subsonic engines such as the one under test.

3. MATERIALS AND METHODS

Field testing for this effort was conducted on 27 and 28 April 2015, at Kirtland AFB in Albuquerque, NM. In coordination with a test stand group at KAFB, tests were conducted by expanding upon a pre-planned operational test sequence for an available engine.

The engine available for testing purposes was a T700-class turboshaft engine, which is typically used to provide shaft power in rotorcraft. While the T700 is not a perfect analogue for high-performance jet engines, as it both produces a less-intense exhaust plume than a turbojet engine would and must drive a shaft and an attached air-resistance turbine while undergoing testing, there remains significant value in conducting testing on this engine. The T700 was physically isolated from the acoustic confounding effects of being attached to an airframe, and the acoustic and infrared background environment at the test stand location was amenable to collecting high-quality data, as the location was in a remote spot surrounded primarily by plain blacktop and empty desert. Additionally, this engine was made available after appropriate coordination, and past extensive efforts to coordinate a test at another location were delayed indefinitely due to exigent circumstances. In the end, it was determined that T700 data would be sufficient for the purposes of this effort, especially since it was deemed unlikely that an engine at another location would be available before the end of a reasonable timeframe for this work.

3.1 Field setup

Figure 2 shows the initial setup. Note the bank of three sensors (SWIR, LWIR, and MWIR) positioned to stare approximately at the expected maximum-emissions zone, about 5- 6 jet diameters away from the exhaust plane. Note the distant microphone, as well as the block used to generate synchronization pulses, placed on a line directly between the instruments and the expected maximum-emissions zone.

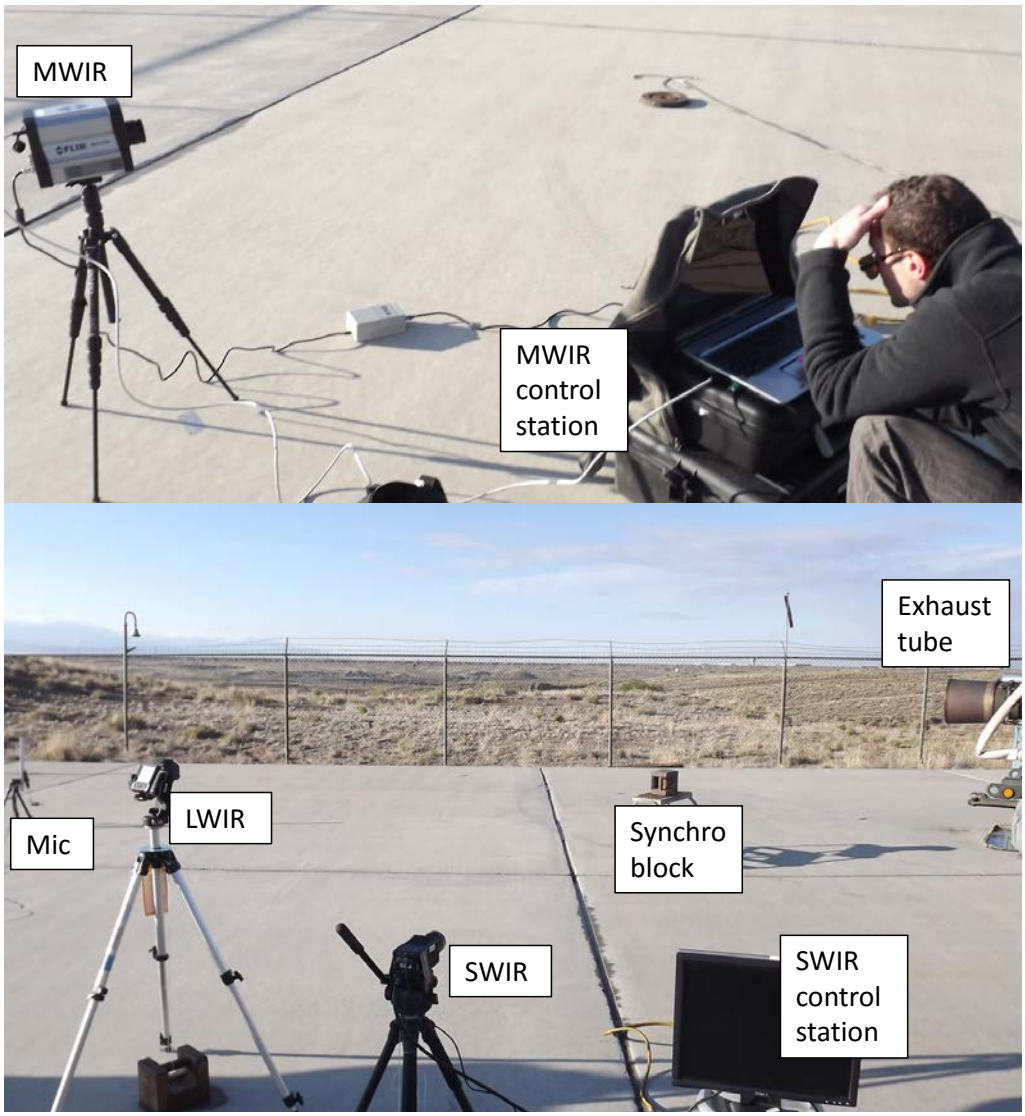

Figure 2. Field test equipment layout.

Figure 3 shows the approximate view cones of the three infrared instruments, as well as the approximate microphone positions, relative to the engine test stand and exhaust axis.

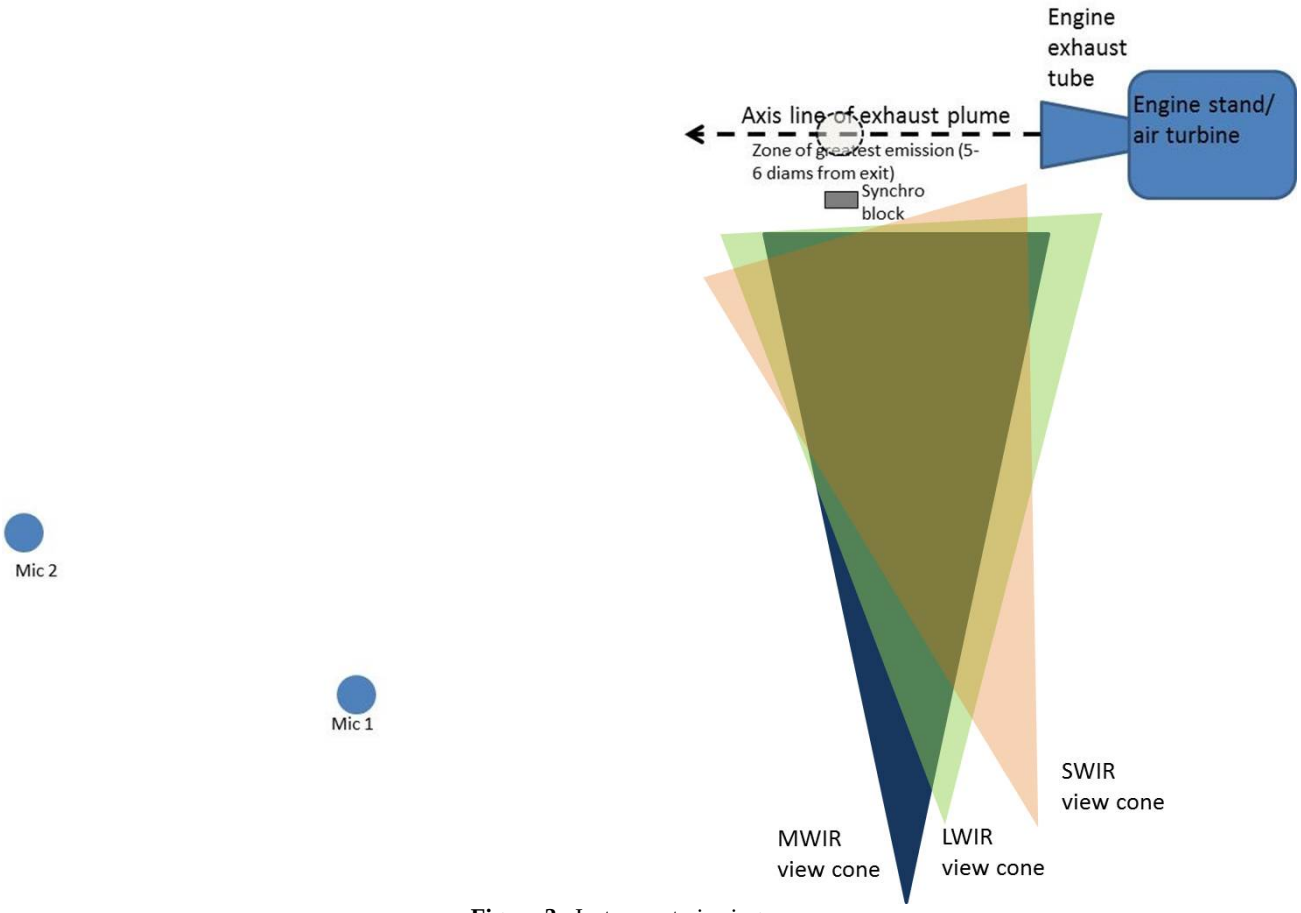

Figure 3. Instrument viewing cones.

Figure 4 shows a closeup of one of the microphone stands, and Figure 5 shows an example of the line of sight of one of the instruments.

Figure 4. Microphone stand setup.

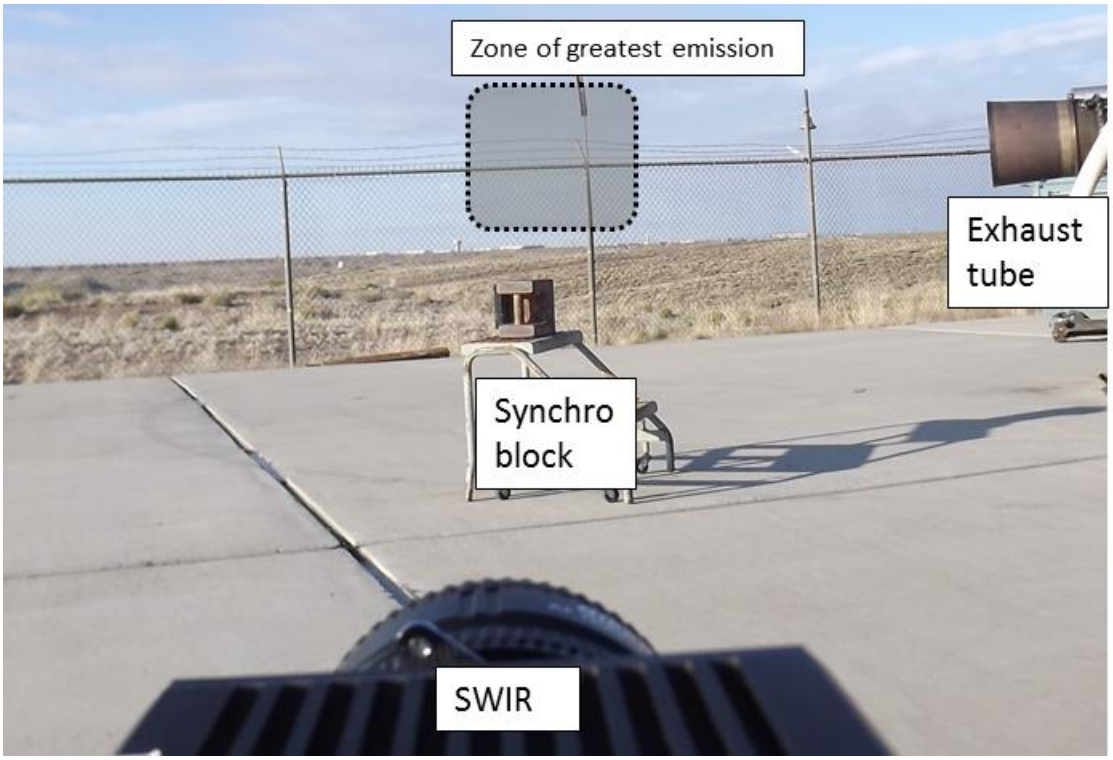

Figure 5. SWIR instrument line of sight.

Note that the predicted zone of greatest emissions is along the physical exhaust axis (and thus above the tarmac), about 5 or 6 jet diameters away from the exhaust plane. Notably, the test area is relatively flat, and thus the exhaust plume tends to flow directly back away from the engine, without creating any noticeable eddy zones anywhere near the instruments. Thus this test produced a relatively clean example of a pure plume in free space, with no notable reflections from an airframe, buildings, or major terrain features.

Figure 6 shows the overall view of the test setup, with the approximate exhaust region marked.

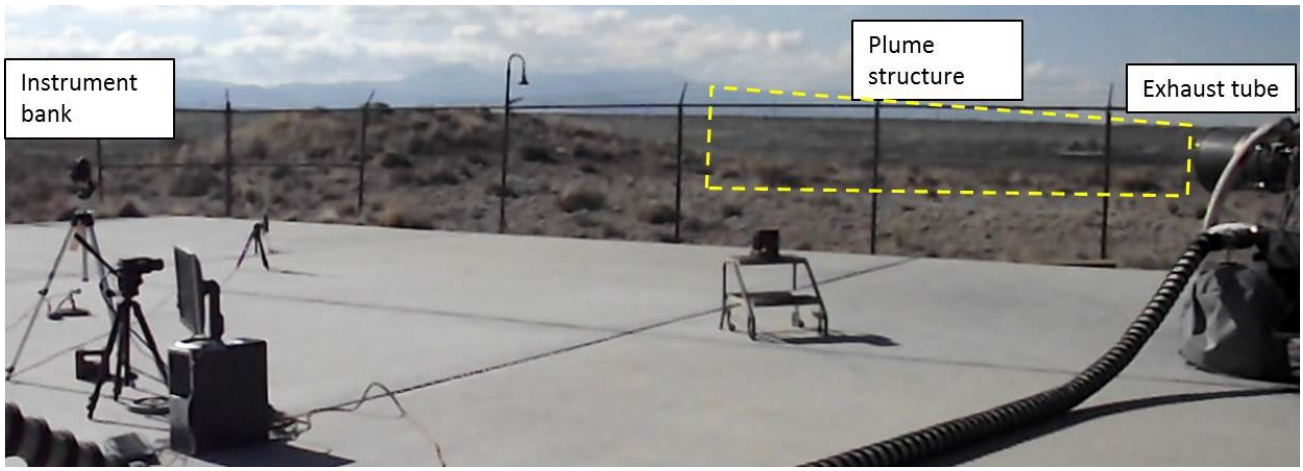

Figure 6. Overall test setup.

3.2 Data collection

Data was collected by folding instrument operations into the predefined engine operations protocol used by the engine test facility at which data was collected. The instruments were placed, and recordings were begun for the acoustic sensors (microphones, of which at any given time two were collecting data), visible context camera, LWIR camera, and SWIR camera. The engine was started and run to an appropriate initial RPM, which entailed a few minutes of run time. Once the engine was ready, a careful throttle profile was run, and test facility personnel activated the MWIR camera to collect data (10 seconds @ 120 Hz – max capture rate) at each new throttle setting. Throttle settings were typically held for 10-30 seconds, and then a ramp up or down to a new throttle setting would be completed.

A given engine run would incorporate from two to four different throttle settings, and would last approximately ten minutes. During this time, all research personnel remained inside a bunker for safety reasons, while test facility personnel operated the engine and confirmed the operation of the scientific instruments used.

At the very beginning of every single engine run, and again at the end, a synchronization pulse event was created, to allow for later precise comparison of the acoustic and infrared data. This event was created by placing several small blasting caps (of the type used in children's toys) on the steel surface of the synchronization block placed in front of the cameras and striking them with a hammer. This produced a short, sharp acoustic pulse, which occurred simultaneously with a short burst of infrared radiation as the caps burned.

Instruments used include a SWIR camera (SU-640, 1.0-1.7 μm), a handheld LWIR camera (mounted to a tripod for this campaign), a MWIR camera (FLIR SC6701, 3-5 μm, 50 mm f/2.5 lens), and two microphones. A visible camera also captured the scene in context.

After an engine run was completed, the research personnel would exit the bunker once given an all-clear, collect data from the scientific instruments, and re-set for another run. Altogether, three engine runs were completed, and data was captured from at least one throttle setting during each of those three runs.

Due to the nature of operations at the engine test facility and the limited scope of this work effort, only one day of data collection was feasible. Repeat operations are a desirable element of future work.

3.3 Limitations

Key operational limitations for this effort included the presence of a large air turbine attached to the T700 engine, the height of the engine above the ground, and the limitations of the cameras used.

The air turbine is a large set of fan blades in a housing to which the T700 engine is connected. The air turbine blades sit in a metal housing directly next to the engine, and the pitch of the blades can be altered by commands from a remote bunker. The net effect is that the air turbine simulates the work that would have to be output from a T700 engine in flight to the main rotor of a vehicle, allowing the T700 on the test stand to experience loading conditions similar to those seen in regular operations. The air turbine generates acoustic noise that is likely unrelated to the noise produced by the engine plume, but which is nonetheless detectable to nearby acoustic equipment.

Another limit imposed by the engine test setup was the fixed height of the engine itself. Since the central flow axis of the engine was forced to reside ~2.5 engine diameters from the ground, it is unclear whether there are significant interactions of the plume dynamics with the ground plane. In general, the following analysis shows great symmetry above and below the central flow axis, especially for high throttle levels, leading us to believe that ground plane effects are minimal. To determine whether the plume dynamics represent those of a free jet, follow-on work could address this issue by examining the cylindrical symmetry of the plume as observed from multiple radial positions perpendicular to the plume.

Additionally, some of the cameras used were unable to collect data for more than a short period of time. For instance, the visible context camera filled its available memory after slightly under ten minutes, resulting in an inability to review visible imagery from the last few minutes of each engine run. This proved largely inconsequential, but the MWIR camera was unable to collect data for more than about 10 seconds at a time, meaning that after the research team performed setup, the test facility personnel were required to restart its data collection for every new throttle setting. This proved less of an obstacle than originally anticipated, as the test facility personnel were able to perform this task effectively after initial training from research personnel. Fortunately, due to the assumed quasi-steady state nature of the plume at each constant throttle level, we do not expect that the analysis results were significantly impacted by this limitation. In future work, we recommend collecting multiple relevant duration measurements at each throttle level in order to verify this assumption. Multiple collects easily could be achieved either by acquiring cameras with expanded high data rate storage, or by using the current cameras with delay times of ~90 seconds between collects while the data is written to hard disk storage.

Additionally, data from the SU-640 (SWIR) camera (cf. Figure 8) did not capture any obvious plume radiation (only reflected background radiation and subtle waves indicative of refractive index changes). We suspect this is due to the blackbody curve shape, with a cutoff exceeding the SU-640's sensitivity band. Using a publicly-available web tool[14] to calculate blackbody curves, with T = 1400 F, the cutoff is seen to be very sharp between about 1.5 um and 2.5 um, leading to no useful data being captured by the SU-640. We do, however, suspect that a higher-power jet engine would produce data visible to the SU-640, as it would be likely to create a hotter plume, which would then radiate more energy in the SWIR bands.

The LWIR data captured was determined not to be useful for quantitative analysis, because the camera captured it as a video file (rather than a pixel-by-pixel data set), and used a constantly-adapting color scale. However, the LWIR data was useful in estimating the temperature of the plume at a fixed location. Figure 7 shows an example of an LWIR image for the engine at idle speed.

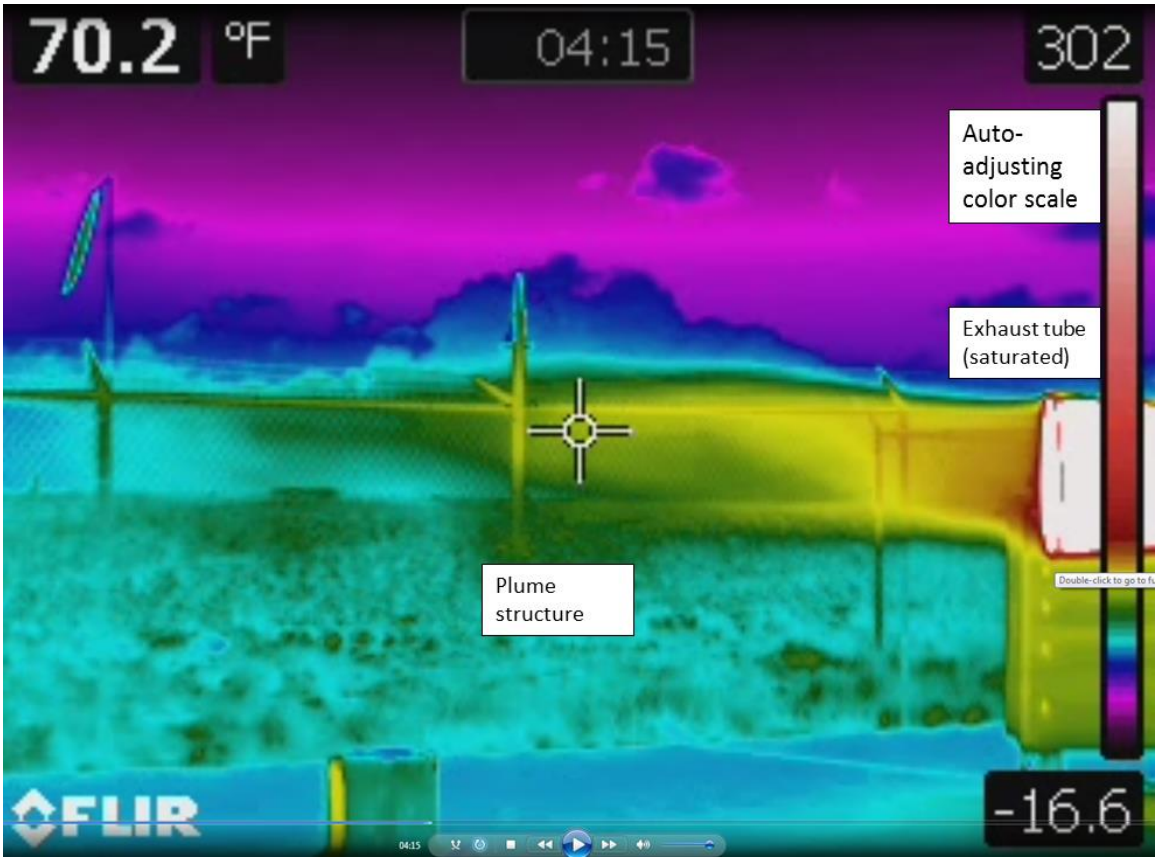

Figure 7. A single frame captured from the LWIR camera.

The LWIR camera used was originally designed as a handheld tool for in-home and other consumer use, and as such does not provide a great deal of scientifically-reliable data. Although, as in Figure 7, some structure is visible in the plume, it cannot be broken down numerically and thus is not amenable to most of the techniques available for fast-framed data analysis. Data from the LWIR camera were accordingly not used for detailed analysis.

Thus, data from the MWIR camera (cf. Figure 9) is used, together with the acoustic data, for most of the analyses described in the rest of this paper.

Figure 8. A single raw frame from the SWIR camera (Speed 3)

Figure 9. A single raw frame from the MWIR camera (Collect 37, Speed 3).

3.4 Test runs conducted

Test runs completed are described in Table 1. Note that at least two data sets from each of four power settings were captured by the MWIR camera (and acoustic sensors), although most of the following analysis focuses on the data sets above idle speed.

Table 1. Test matrix for planned field campaign. Sensor locations are as in Figure 4.

Collect #	Engine throttle profile	Mic location	Notes
35	Idle (speed 1)	1, 2	120 Hz, 1200 frames, turbine temp 861
36	Intermediate (speed 2)	1, 2	120 Hz, 1200 frames, turbine temp 1007
37	Fly (speed 3)	1, 2	120 Hz, 1200 frames, turbine temp 1108
40	Idle (speed 1)	1, 3	120 Hz, 1199 frames, includes re-cal, turbine temp 855
41	Intermediate (speed 2)	1, 3	120 Hz, 1200 frames, turbine temp 1007
43	Fly (speed 3)	1, 3	120 Hz, 1200 frames, turbine temp 1127
43	Full (speed 4)	1, 3	120 Hz, 1200 frames, turbine temp 1600
45	Full (speed 4)	1, 2	120 Hz, 1200 frames, turbine temp 1596

Altogether, these tests were intended to capture acoustic and infrared data from a variety of situations, increasing the likelihood that, if correlations between acoustic and hypertemporal infrared emissions exist, they would be captured.

3.5 Data processing plan

The planned field campaign was expected to produce several data sets of time-tagged acoustic and infrared data. These data sets were processed (PCA was applied to the infrared data), and the presence of any hypertemporal characteristics, such as unique power spectral distributions, was. Additionally, the presence, absence, or changing of hypertemporal characteristics, as well as the precise characteristics themselves, in the infrared regime was able to be compared to the SPL recorded and the engine throttle settings.

This effort was intended to search for the presence of such correlations; as such, any identification of such a correlation can be considered a successful result for the field campaign.

4. RESULTS AND DISCUSSION

Several analyses aimed at understanding first the IR data, then the acoustic data, then the relationship between the two, were conducted. Ultimately, strong correlations were observed between simultaneous MWIR and acoustic measurements.

4.1 Spatial correlations within MWIR data

In order for the MWIR data to be best understood in combination with the acoustic data, we worked to understand the characteristics of the MWIR data itself. The following analysis aims to reveal the

underlying spatial structure of the engine plume as captured in the MWIR. Such analysis makes use of principal components analysis, which separates correlated signals into orthogonal image projections. In this way, underlying temporal correlations can be made manifest in the spatial domain.

Analysis Goal: Determine spatial regions of temporal correlation.
Analysis process for generating the following figures:

1. Perform principal components analysis on video data in order to separate orthogonal sources of IR fluctuations.
2. Project a single principal component video stack (pixels with correlated time histories)
3. Calculate the RMS AC signal of each pixel time history, and display the resultant single AC image (cf. Figure 10).

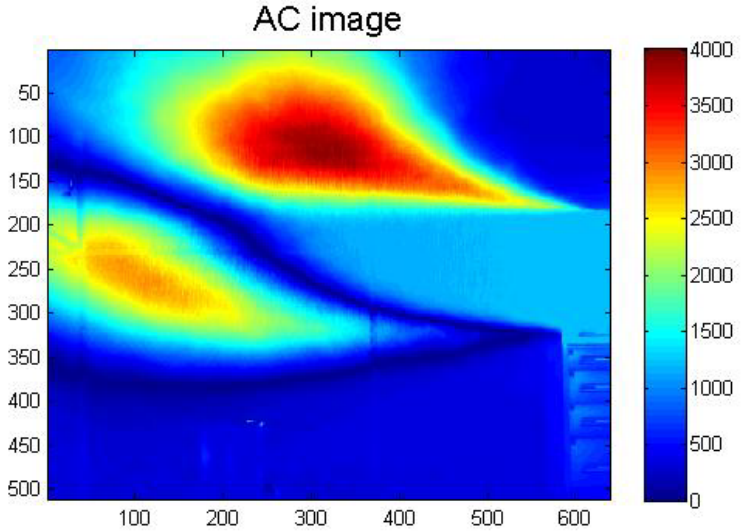

Figure 10. AC image of PC 2 in MWIR for #35 data run, at idle (speed 1).

In order to help interpret these plots, consider Figure 10, which shows some plume structure for the second principal component of the #35 data run. Note that the central plume is saturated (the light blue region to the right), while there are visible both an upper curve and a lower curve (two red/yellow regions) to the left. The line between the two fluctuating regions represents a line of nodes which experiences less variation overall. Viewing a video of the second principal component quickly reveals that the maxima shown in Figure 10 indicate regions of IR energy transfer. That is, IR intensity switches several times between the upper and lower maximum of Figure 10. This indicates that adjoining maxima in the AC images may be considered as regions of correlated energy transfer.

Figure 11 again shows principal component two, but for the high-power case (#43 data run, speed 3). The plume structure is again present, but the plume leans straight back rather than curving up (reflecting most likely a higher exhaust speed at this throttle level). Here, two regions of correlated energy transfer appear to be shifted farther away from the engine nozzle, as may be expected for a higher speed plume with more rigidly defined structure.

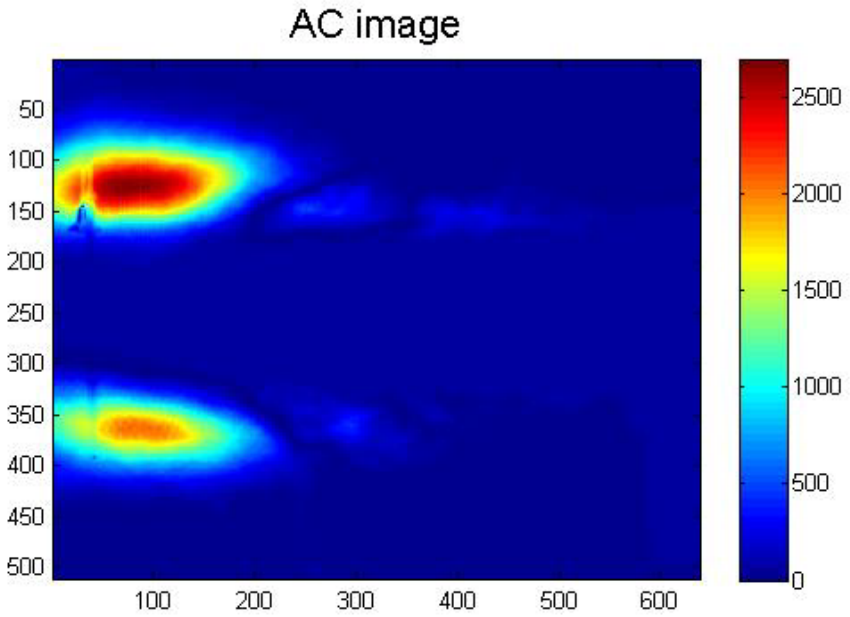

Figure 11. AC image of PC 2 in MWIR for #43 data run.

Comparing figures reveals that plume structures change in size as throttle levels rise. This is easily seen in Figure 12, which compares principal component 2 for varying engine throttles. Furthermore, by viewing additional principal components, images which separate orthogonal correlations, additional features appear that make it clear we observed a highly complex fluid flow (Figures 13-16).

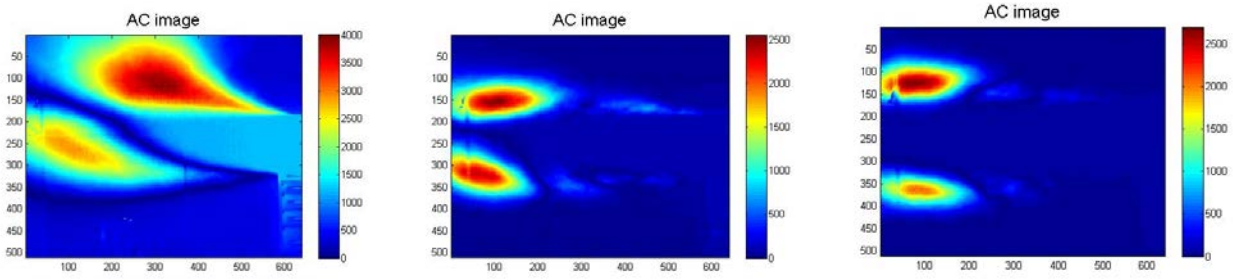

Figure 12. AC images of PC 2 in MWIR for multiple data runs (left to right: idle, intermediate, full speed).

Throughout Figures 13-16, we observed that as the PC number increases, the number of correlated energy transfer regions increases and the maximum AC value decreases. Nonetheless, even in the last principal component (1200) we saw evidence of real structure with significant AC contribution to the overall MWIR signal. The remainder of this report gives insight into what these regions of correlated energy transfer may and may not indicate about the generated acoustic field.

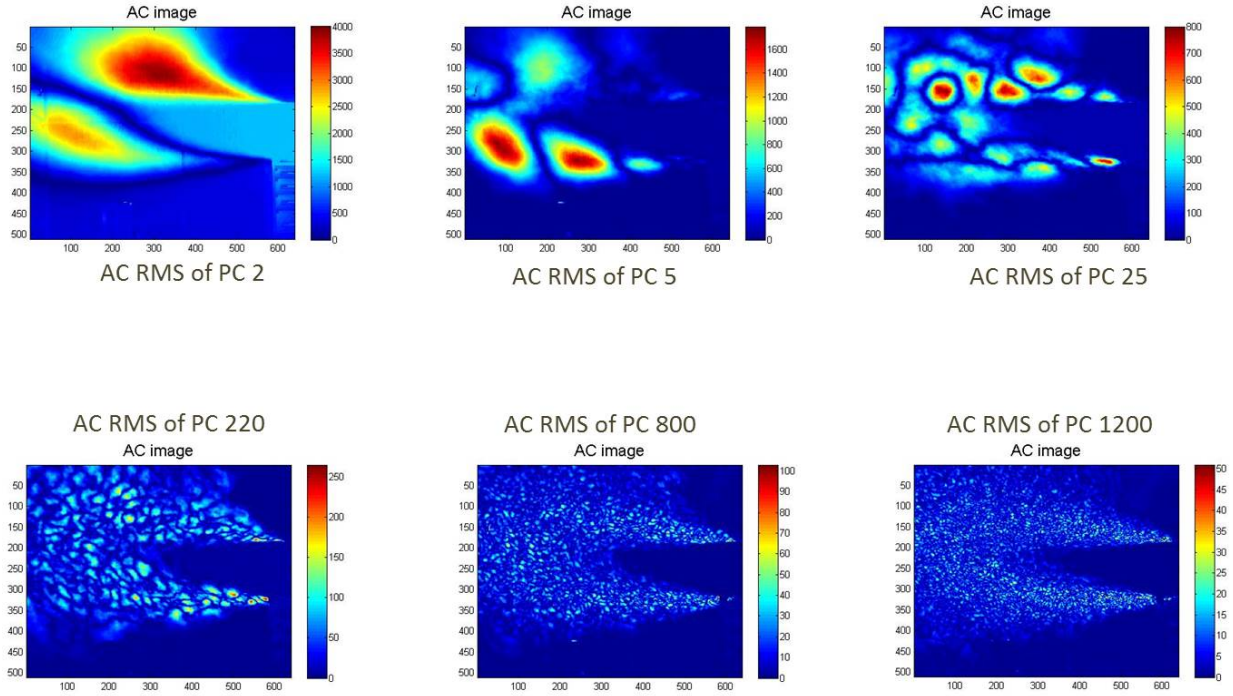

Figure 13. Rec 35 (Speed 1): AC RMS of principal component projections.

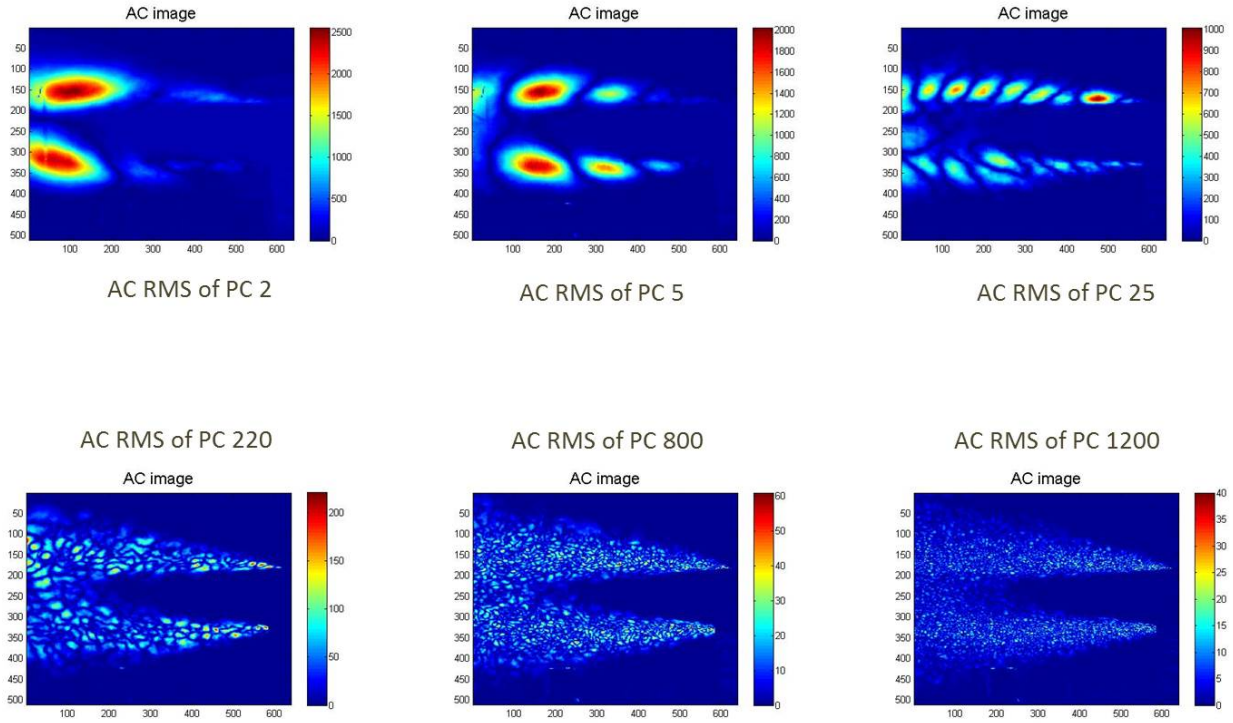

Figure 14. Rec 36 (Speed 2): AC RMS of principal component projections.

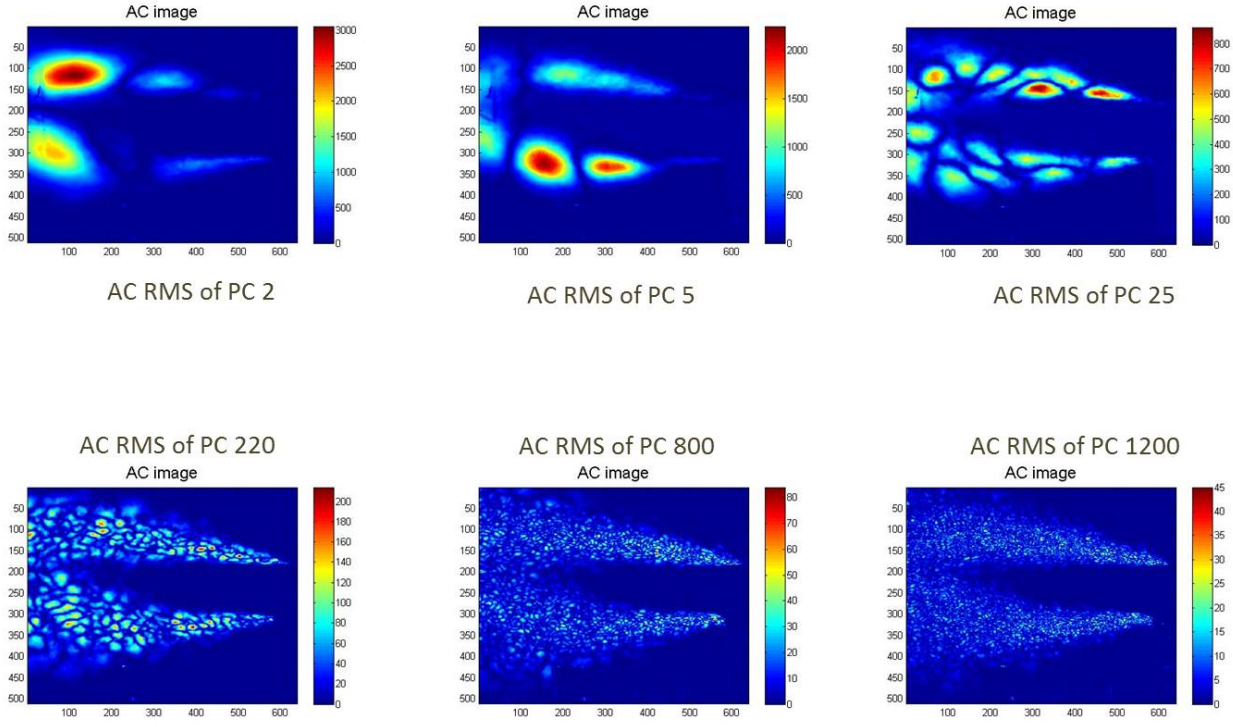

Figure 15. Rec 37 (Speed 3): AC RMS of principal component projections.

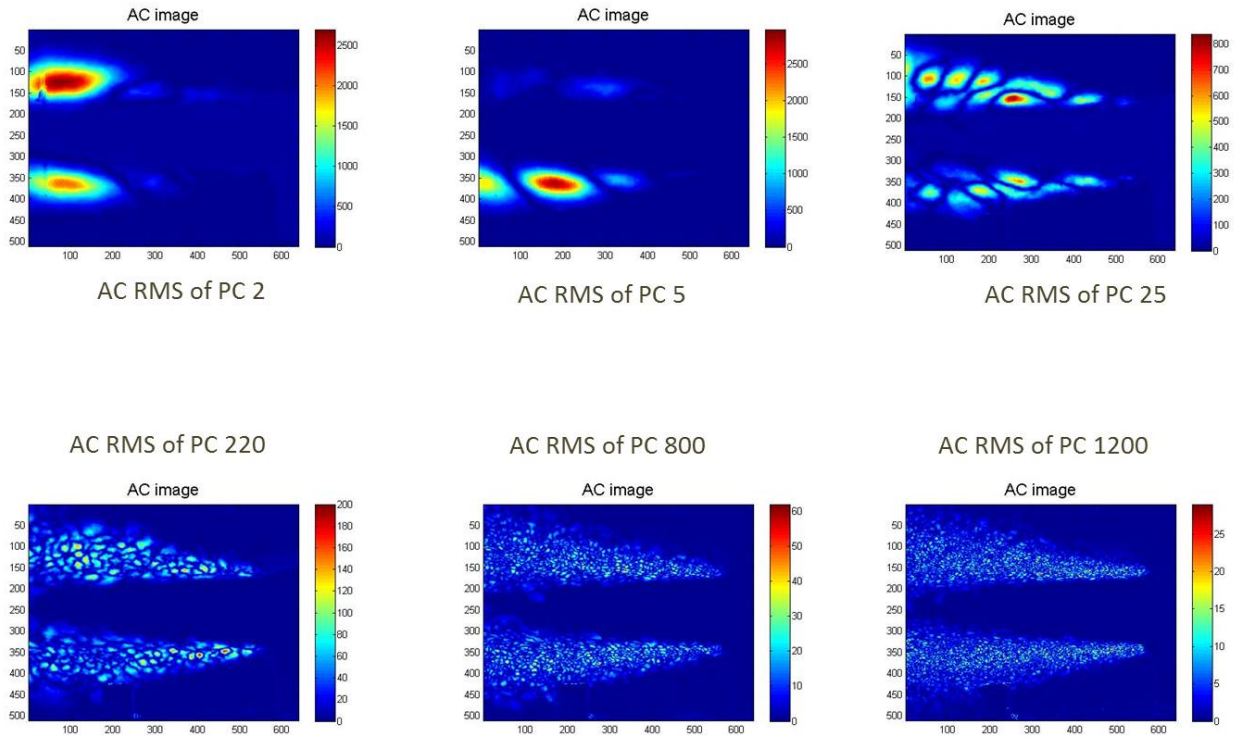

Figure 16. Rec 43 (Speed 4): AC RMS of principal component projections.

4.2 PSD analysis

The principal components captured by the examples of Figures 13-16 suggest more than 1200 different correlated signals captured by the MWIR camera. One interpretation of this could be that each component captured a significantly different temporal signature. For comparison here, we interrogated the power spectral density (PSD) expressed by different principal components and looked for indications of directly related acoustic phenomena.

Analysis Goal: Determine differences in temporal PSD signature indicated by different principal components.
Analysis process for generating the following figures:

1. From the AC RMS image of a specific principal component, find the pixel with the maximum AC RMS.
2. For that pixel, retrieve its time history from the video stack of that principal component.
3. Generate the PSD of that pixel time history (which is representative of the PSD for each pixel time history in that stack – because of the correlation required by principal components analysis).

Figure 17 shows the plots of power spectral density which are characteristic of different principal components at each engine throttle level. In general, the lower principal components exhibit a high frequency roll-off, but beyond this observation early results for this effort have not been promising,

as there is no immediately apparent feature of the PSD in the infrared data which obviously corresponds to a strong acoustic feature. (This feature, if present, would presumably manifest as a spike in the PSD at a frequency known to be the same as, or perhaps a harmonic of, an acoustic frequency with strong emissions.) It may be that this analysis requires more subtle interpretation, including: 1) calculations of the correlation with acoustic data (cf. Section 5.4); 2) interrogation of the spectral phase indicated by each principal component; 3) reliance upon higher frame rate MWIR imagers.

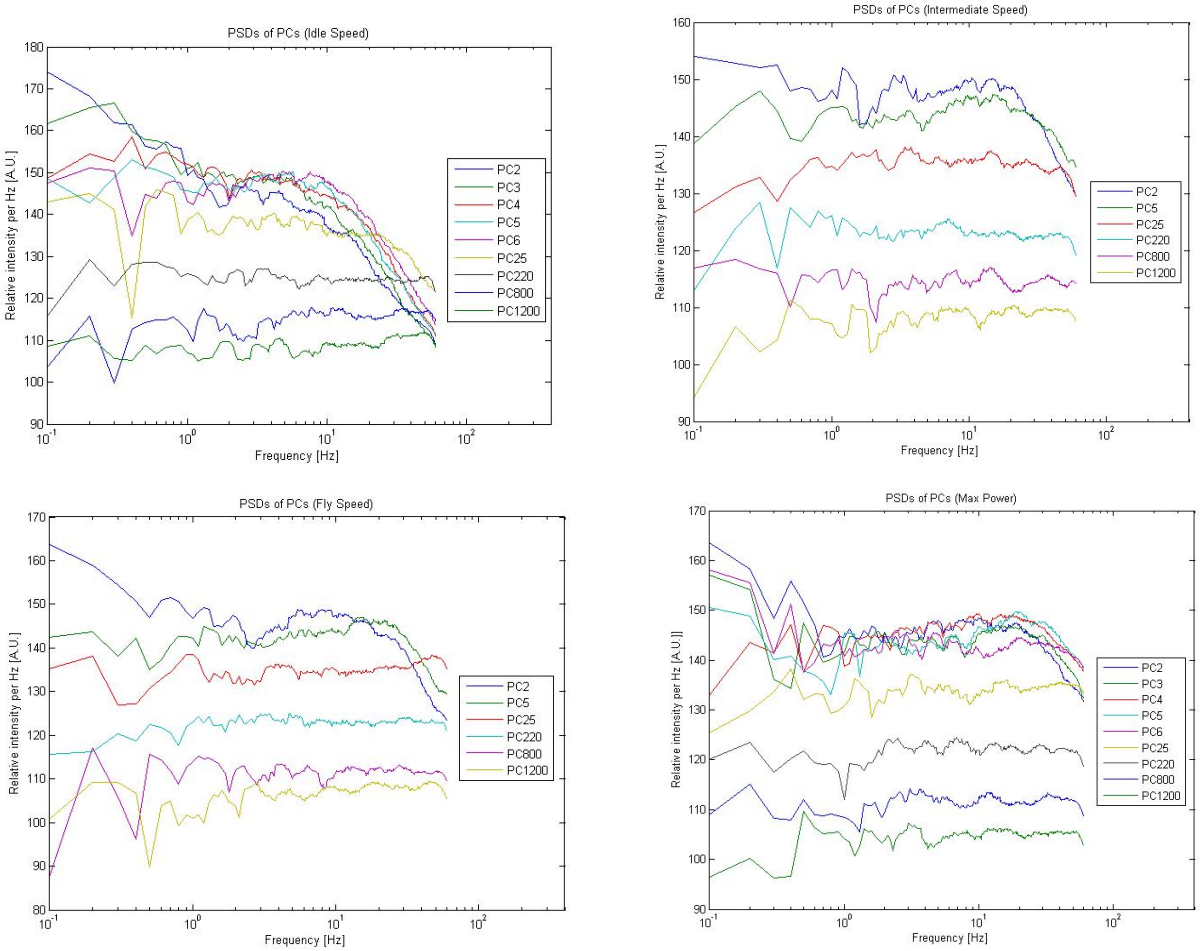

Figure 17. PSDs of different principal components at each level of engine power.

4.3 Analysis of acoustic data

Initial analysis of acoustic data was done using the second data run, as illustrated in Figure 18. This acoustic data run covers multiple infrared data runs, across all four throttle levels of the turboshaft engine.

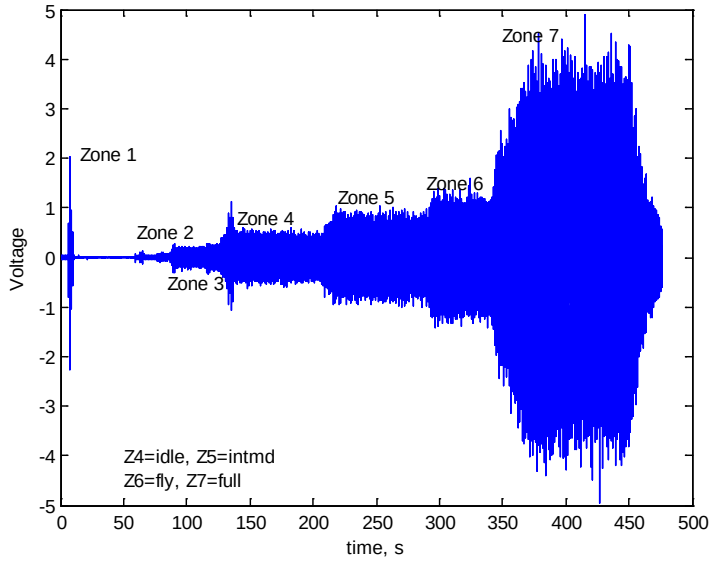

Figure 18. Acoustic data.

Note that the file was truncated at around 475 seconds – there is another ramp up following this. The data seen here show seven "zones" – time periods where there is a noticeable steady pattern in the data. Zone 1 is the firing of the caps for data synchronization purposes, and occurs very briefly and very early. Zone 2, after a lull of some time, includes a very low level of noise, and is followed by the slightly-higher Zone 3. These are believed to be the early start-up and warm-up to idle of the T700 turbine. There is a short spiky region at the boundary between Zone 3 and Zone 4 – this may be some transient related to turning off the supporting equipment attached to the T700 engine, or starting up the ancillary load-creating air turbine. Nonetheless, Zone 4 is identified as the "idle" thrust level of the turbine, corresponding to Speed 1 as identified in Table 1. Following this, Zone 5 is the "intermediate power level," corresponding to a high turbine rpm but a low load on the air turbine/rotor emulator, or Speed 2. Zone 6 is the "fly" power level, corresponding to the situation expected to occur when the helicopter is in standard airborne operation, at Speed 3. Finally, the noticeably-louder Zone 7 is the full power level, or Speed 4.

We confined our analysis to these four loudest zones (Zones 4, 5, 6, and 7), corresponding to each of the four engine speeds tested. The figures below show pressure spectra (sound pressure levels across frequencies, with a total SPL listed at the top) on the left, and spectrograms (sound levels over a thin slice of time during that zone era, at various frequencies, with darker red indicating more power) on the right.

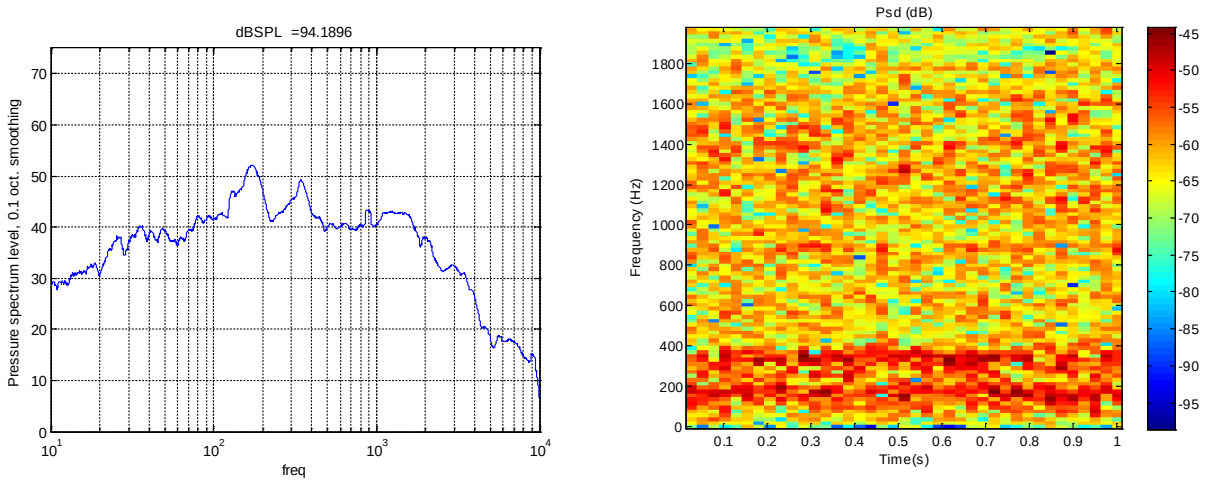

Figure 19. Zone 4. Idle power/Speed 1.

Note that there are frequency peaks in Zone 4 at just below 200 Hz and about 350 Hz. These are the high spikes on the left plot, and the red peaks across the bottom of the right plot. Weaker peaks near 900 and 1000 Hz are also seen.

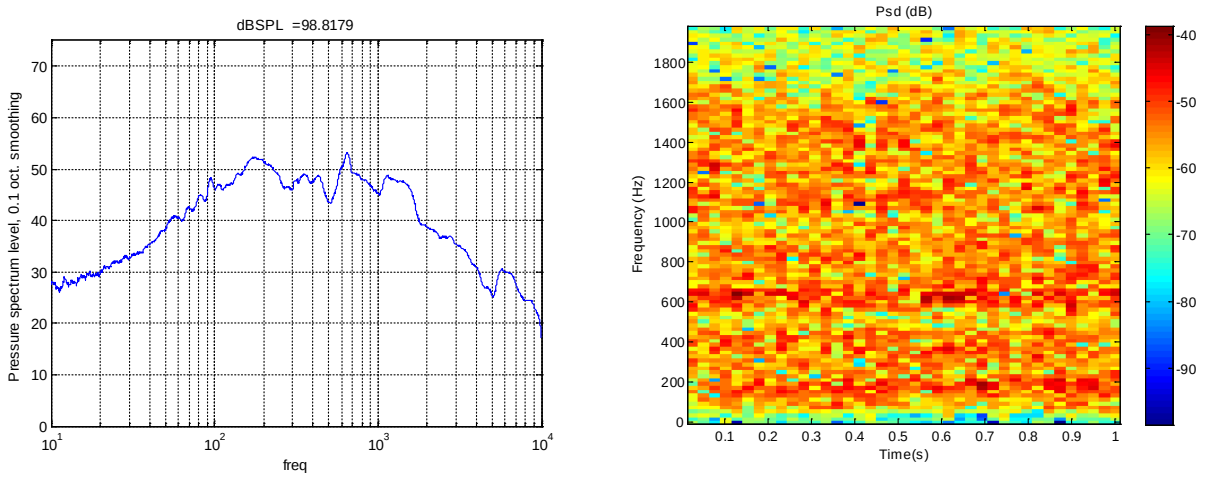

Figure 20. Zone 5/Intermediate power/Speed 2.

Note that the same peaks at 200 Hz and 350 Hz are present, and while the peak at 350 Hz is beginning to weaken relative to the other peaks, the peak at 1000 Hz has strengthened, and there is another peak growing at around 650 Hz.

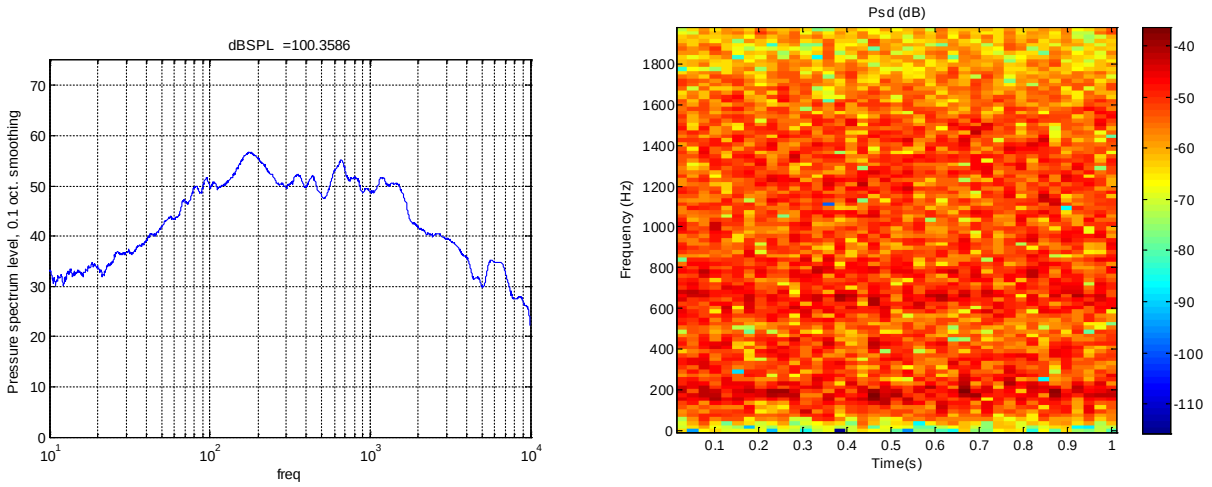

Figure 21. Zone 6/Flying power/Speed 3.

Here, we see that the peaks at 200 Hz and 650 Hz have strengthened further, although the peaks at 350 Hz and 1000 Hz remain present. The shape of this peak remains very similar to the Zone 5 peak, albeit raised in magnitude.

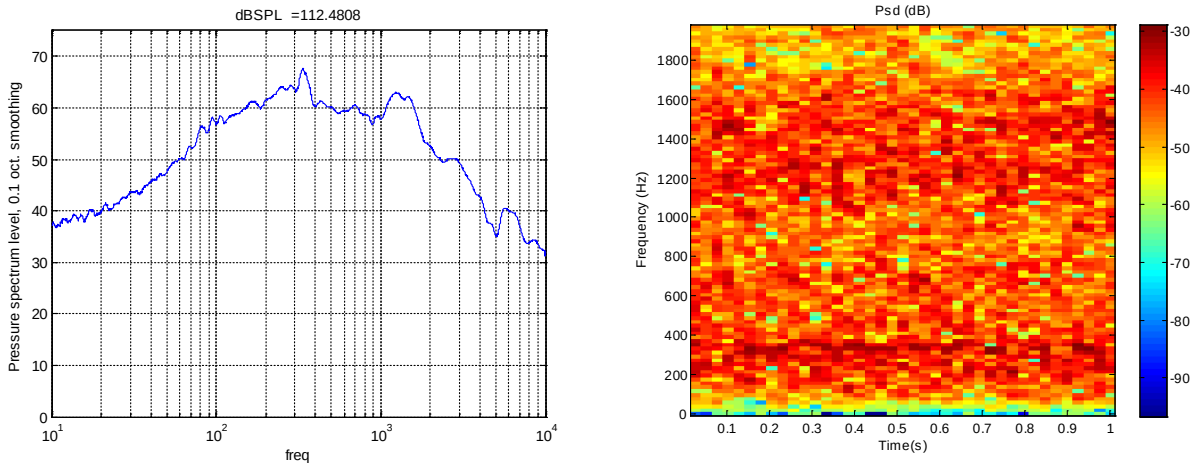

Figure 22. Zone 7/Full power/Speed 4.

In Zone 7, the magnitude of the entire curve has once again grown, but the shape is changed (especially the relative spikes). The peak at 350 Hz and the peak at 1000 Hz now dominated over the weaker (but still present, and in absolute terms somewhat stronger) peaks at 200 Hz and 650 Hz.

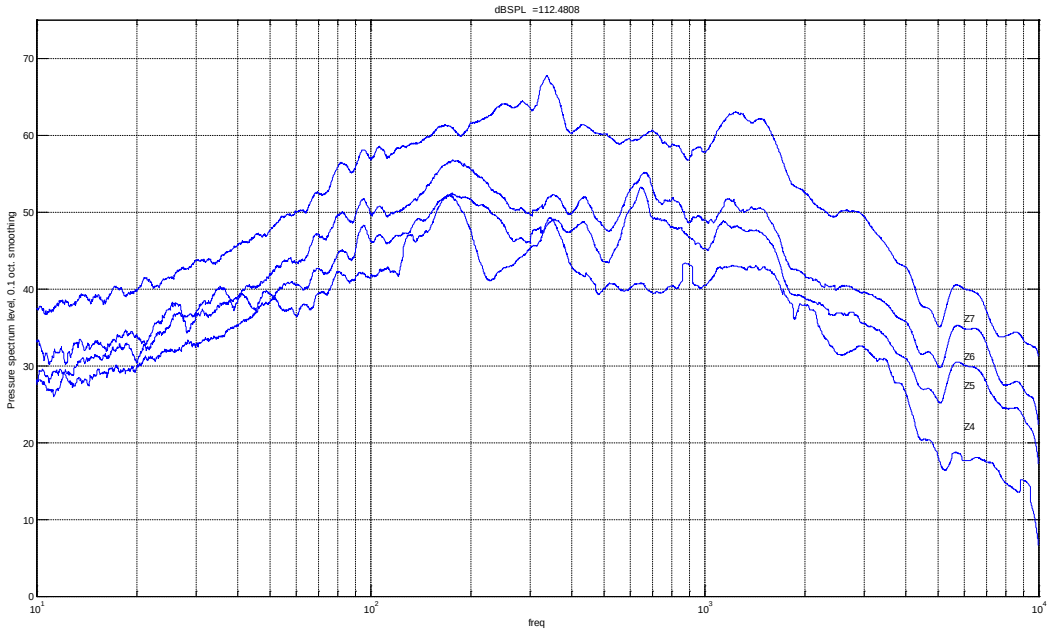

Figure 23. Acoustic data across four noise zones.

One last instructive figure is seen above, showing all four curves (roughly in ascending order of power level from bottom to top; note markings on the far right), taken from data collected only during each zone era.

There is a definite spike structure to the curves, even as they ascend in absolute value. Spikes appear at below 200 Hz, about 350 Hz, transiently near 650 Hz, and very broadly at just over 1000 Hz. There is also a (much lower) spike seen at around 6000 Hz, which may be a harmonic of some kind.

In general, there is some apparent structure in the acoustic noise, and there is also evidence of features of this structure changing as the throttle settings change. While all this is to be expected, any correlation detected between this and the hypertemporal structure detected in the plume may show how the two are related. Unfortunately, all of the most prominently observed acoustic features lie outside the range accessible by the imagers employed for this effort. Still, some correlations were observable, as outlined below.

4.4 Mapping correlations between MWIR and acoustic data

Perhaps the most interesting structure was seen by mapping correlations between the acoustic data and the raw MWIR data. Figures 25-28 show these results.

Analysis Goal: determine the correlation relationship between IR and Acoustic data and plot it spatially.
Analysis process for generating the following figures:

1. Low pass filter the acoustic data to match Nyquist sampling in the video data.
2. Take the filtered acoustic data and extract the samples synchronized with the video data as shown in the timing diagram of Figure 23.

3. Mean-subtract the acoustic data and each pixel time history in the video data.
4. For each pixel in the video data: calculate the covariance of the pixel time history with the acoustic data.
5. Generate a covariance map (indicating relative strength of direct and inverse correlation) from the values calculated in step 4.
6. Optionally: Repeat steps 2-5 with different synchronization offsets to allow for different locations of sound generation within the plume. The overall level of correlation may be approximated by taking the sum of the absolute value of each pixel in the covariance map.

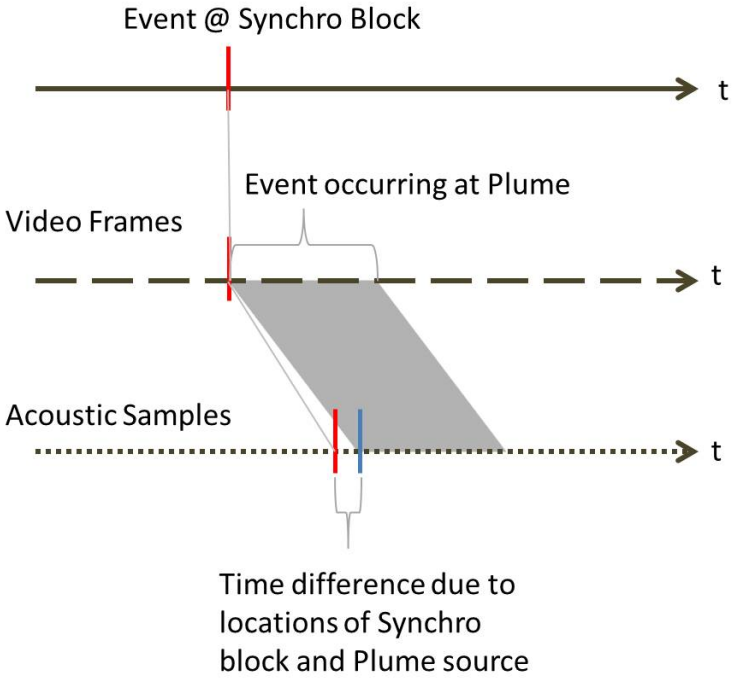

Figure 24. Timing diagram for synchronization of video and acoustic data.

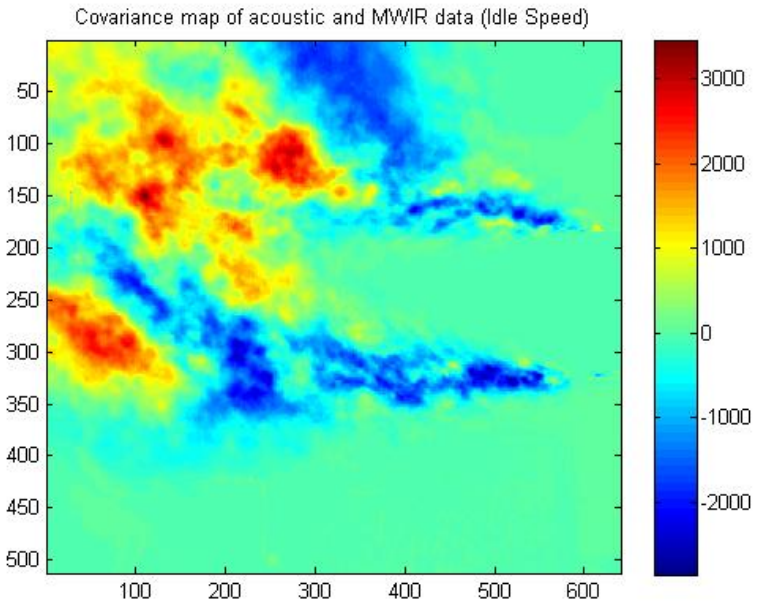

Figure 25. Covariance map at speed 1

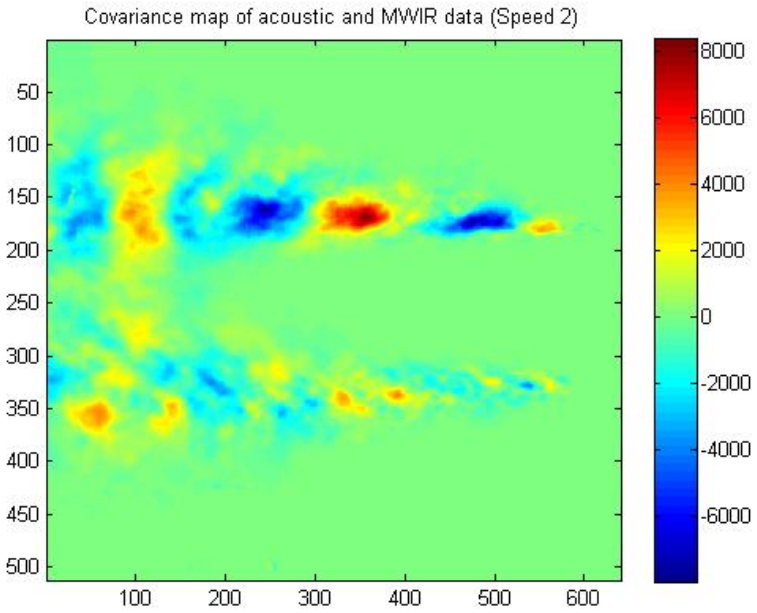

Figure 26. Covariance map at speed 2

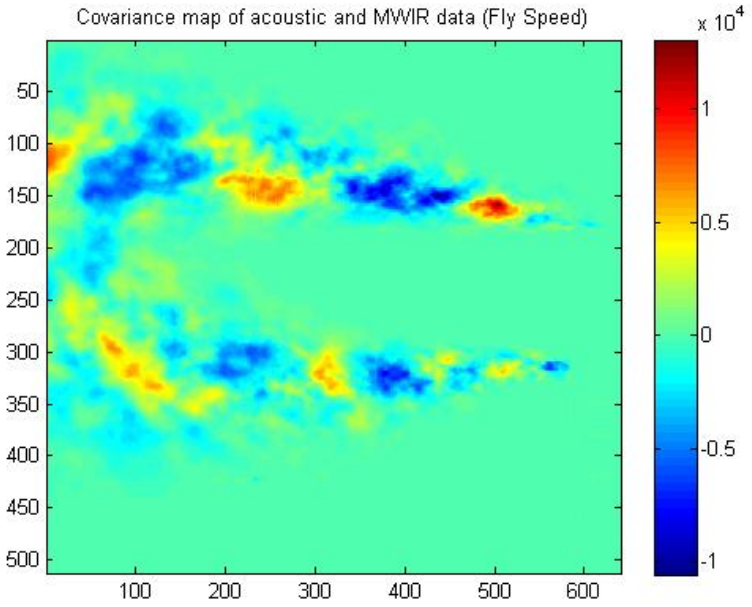

Figure 27. Covariance map at speed 3

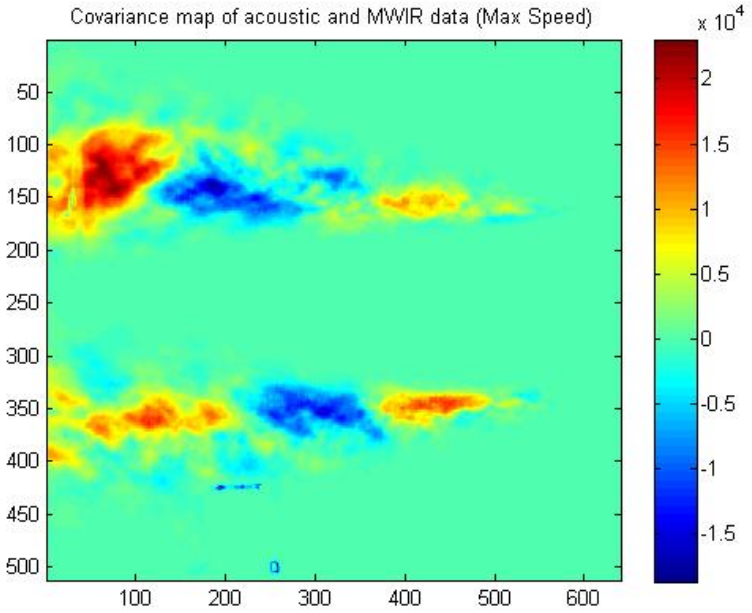

Figure 28. Covariance map at speed 4

Note that both the engine speed and the value of maximum covariance increases from Figure 25-28. Throughout Figures 25-28, red areas indicate high direct correlation, the blue areas indicate high inverse correlation, and the green areas indicate near-zero correlation. As expected, there was no correlation between MWIR and acoustic data either outside the plume or in areas in the center of the plume where the MWIR camera saturated.

Notably, the plume straightens out as speed increases, and begins to take on a pattern of alternating direct and inverse correlation regions, all of which shrink as the speed goes higher. This is possible evidence for wave packets moving across the field of view, since neighboring direct and indirect correlations may likely indicate a transfer of IR energy between the regions.

Viewing these figures in light of the principal components images of Section 5.1, striking similarities make it appear that the regions of highest correlation coincide with the energy transfer processes captured by principal components between 5 and 25. Additional temporal resolution in the MWIR imagery may be of critical need to help explain why this is the case given the murky results of initial temporal analysis shown in Section 4.2.

Further work, to capture more data and perform more detailed analysis, is suggested. Ideally, future work would use a much faster-framed imager in the MWIR, one that may allow clear temporal signatures to be distinguished along with tracking the interframe motion of plume structures.

4.5 Possible explanation of results

It may be that the changing correlation structure is indicative of a physical phenomenon. However, future work to determine the exact mathematical relationship of such a correlation is desirable – many tests, at a wide range of finely-calibrated engine speeds, may now be prescribed. This could produce statistically reliable estimates of how the emitted sound spectrum varies with the temporal signature of infrared principal components.

If this relationship is found to hold true across an extended range of operational conditions, it may be possible to estimate acoustic frequencies emitted, or what mix of peaks is emitted, from a simple MWIR principal component image of the engine.

4.6 A surprising potential application

One interesting side analysis conducted incorporated an assessment of the optional analysis step (#6) of Section 4.4. To verify the location of the center of maximum acoustic emissions, suspected to be at 5-6 diameters from the exhaust plane, the aggregate value of each pixel's correlation strength was calculated and summed. Then, to account for acoustic delay, the assumed distance from the center of acoustic emissions was varied in increments of 1 foot from -6 feet to 40 feet. Using the filtered acoustic data and MWIR measurements, the resulting aggregate strength of the correlation was plotted (Figure 29), and it was seen that the maximum-strength correlation occurred at 27.5 feet. A precise interpretation of these data is not easily made; however, more work on this particular analysis may enable one to calculate the location of maximum acoustic generation, potentially even as it moves around a spatial region.

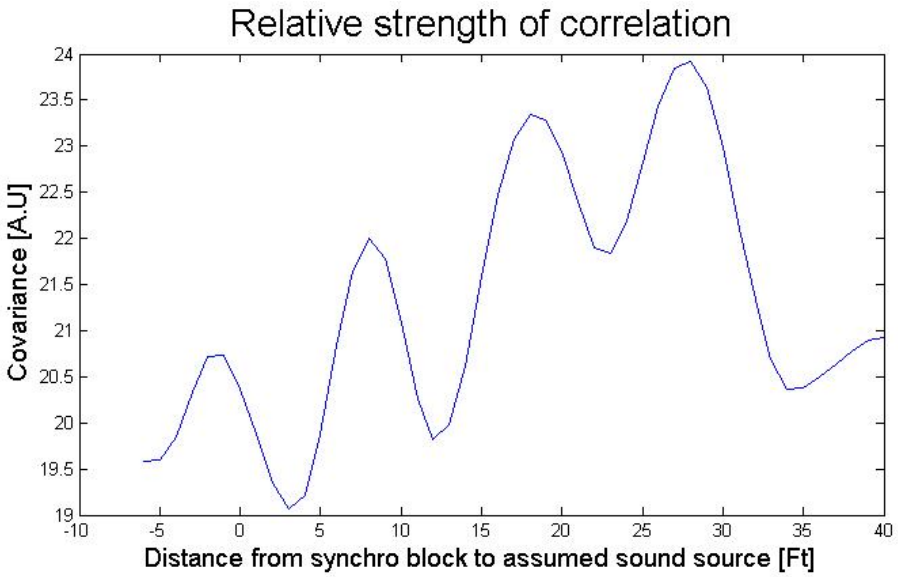

Figure 29. Relative strength of correlation between MWIR and acoustic data for varying temporal offset (Rec 37, speed 3).

The application of this is as follows: if an infrared image of an exhaust plume can be captured and processed with appropriate temporal algorithms, then it could be simply convolved (via a dot-product) with a matrix of expected acoustic emissions, perhaps a spectrum weighted to capture the frequencies most damaging to human hearing. The processing of this imagery would then indicate where precisely the most-damaging physical spots for human hearing were located, and could potentially detect them dynamically, without the use of microphones.

Proving this application would require extensive additional work to verify that the apparent location of the center of maximum acoustic emissions is actually being detected, and that the relationship between acoustic and infrared emissions holds at various power levels and under various geometries for various engines, so that centers of acoustic noise could be accurately tracked in space and time. However, if viable, this application may be used to coordinate flight-line operations in a way calculated to protect human hearing, using only remote imaging and processing.

5. CONCLUSIONS

Analysis of simultaneously acquired acoustic and IR measurements of a T700 engine under test yielded several notable conclusions relevant to using hypertemporal imaging techniques to aid in mitigating jet engine noise generation.

An analysis of MWIR data alone indicated the specific structure of correlated energy transfer processes within the engine plume down to significantly small spatial scales and at significantly small AC contributions. Such fine resolution may be very useful by itself as truth data for refining computational fluid dynamics models used when designing jet engines. Such additional refinement may lead to greater success in mitigating jet engine noise via design.

Direct analysis of the acoustic data indicated that the most prominent noise features are present at frequencies beyond the frame rate capabilities of the IR imagers used in this analysis. However, IR imagers with adequate frame rates (>500 Hz) do exist and may now be acquired for future work based on this analysis.

Of most significance here, the analysis incorporating both MWIR and acoustic data indicates regions of high correlation with clear structure. In this way, at least some of the dynamics of the engine plume that are responsible for acoustic generation are clearly captured by IR observations. Viewed in light of the principal components images of Section 5.1, striking similarities make it appear that the regions of highest correlation coincide with the energy transfer processes captured by principal components between 5 and 25. If these processes can be both understood and separated from non-noise generating flow, the mitigation of such processes could be prioritized when designing quiet jet engines.

The next steps for expanding on each of these results rely upon repeated trials with higher frame rate IR camera observations of more relevant engines under a range of operating conditions.

6. IMPLICATIONS FOR FUTURE WORK

This work met the success criteria originally described in Section 1 of this report: hypertemporal signatures were found in jet engine infrared plumes (in the form of correlated regions of energy transfer), and initial evidence was found that there is a correlation with acoustic signatures (in the form of correlated relationships between the time history of pixels and the acoustic time history).

Now that the presence of and relationship between hypertemporal and acoustic emissions is established, follow-on efforts to this work should be shaped to provide better resolution of the acoustic and IR fields in both time and space. This is readily accomplished by using both additional microphones in appropriate configurations and faster framing infrared detectors. For instance, while this work focused on acoustic emissions primarily from a single location - the strongest acoustically emitting region in the jet plume - techniques exist to determine relative contributions of noise sources along an axial line.[13] Application of these techniques may enable future work to distinguish between various acoustic emissions sources to a great degree. When coupled with enhanced IR observations (e.g. up to the 43 kHz frame rates of a FLIR SC4000), much more detailed analysis is enabled for characterizing the underlying processes indicated by acoustic and IR correlations. While it would be an expansion from the scope of data collection alone, any follow-on work would also benefit greatly from closer collaboration with CFD modeling subject matter experts.

Accordingly, a repeat field campaign is a highly desirable future work effort. Ideally, this field campaign would take place with the following advantages over the one conducted in this initial effort:

1) Improved instrumentation – the use of infrared cameras with high frame rates (and, if possible, sufficiently high dynamic range to avoid having regions of the plume saturate), as well as the use of advanced acoustic sensing arrays scattered over a wide physical area to allow for possible analyses of the plume as a string of emissions sources, would allow for more fine-tuned data collection in the acoustic and thermal domains.

2) A more isolated turbine engine – it was difficult to identify and explicitly account for the effects of the air turbine connected to the T700 turboshaft in this effort. Future work would ideally incorporate only a turbine engine, leaving a potential major confound to the results entirely out of the environment where data is collected.
3) A higher-power turbine engine – although the T700 engine does produce a plume and operate in a manner similar in general ways to other high-performance turbines, it does not function precisely as a high-performance turbojet or turbofan engine would, and therefore it is not immediately clear to what extent the results of this effort may extend to turbofans and turbojets, which are very powerful acoustic noise emitters.

Another key element of future work will thus be obtaining the necessary facilities and time to operate an appropriate engine under a wide range of conditions, including various throttle settings. Although the initial work done here indicates that correlations are present in some way, it would be useful to determine how they might evolve over time as an engine is operated for an extended period.

Finally, much more in-depth analysis of results should be done to assess to what extent the existence of peaks and valleys in acoustic and infrared correlation (as indicated in Section 5.6) is indicative of real physical phenomena, and to what extent it may be artifactual. Using other means to verify that regions of maximum acoustic noise emission have moved in physical space (such as acoustic array sensors), potentially in concert with flow visualization techniques such as smoke streaming, could be used to take additional data on the physical and acoustic structures present in a standing plume, and to attempt to strengthen the correlations visible between these and infrared imagery as analyzed by principal component techniques.

REFERENCES

[1] Bogey, Christophe, Bailly, Christophe, and Juve, Daniel, "Flow Field and Sound Radiation of a Mach 0.9 Jet Computed by LES," RTO AVP Symposium on Ageing Mechanisms and Control: Part A – Developments in Computational Aero- and Hydro-Acoustics (2001).
[2] Casalino, D., Diozzi, F., Sannino, R., and Paonessa, A., "Aircraft noise reduction techniques: a bibliographic review," Aerospace Science and Technology (2007).
[3] Möser, M. and Müller, G., [Handbook of Engineering Acoustics], "Fundamentals" chapter, Springer-Verlag, Berlin and Heidelberg (2013).
[4] Grosveld, Ferdinand W., Sullivan, Brenda M., and Rizzi, Stephen A., "Temporal Characterization of Aircraft Noise Sources," 42nd Aerospace Sciences Meeting and Exhibit (2004).
[5] Michel, U., Dobrzynski, W., Splettstoesser, W., Delfs, J., Isermann, U., and Obermeier, F., [Handbook of Engineering Acoustics], "Aircraft Noise" chapter, Springer-Verlag, Berlin and Heidelberg (2013).
[6] White, Jack R., "Aircraft Infrared Principles, Signatures, Threats, and Countermeasures," Naval Air Warfare Center Weapons Division Technical Paper NAWCWD TP 8773 (2012).
[7] Ogg, Jack W., "Detection of Aircraft Engine Configuration via Exhaust Radiance Temporal Modulation," Naval Postgraduate School MS thesis (1990).
[8] Sinha, N., Ungewitter, R. J., Kenzakowski, D. C., and Seiner, J. M., "Gas Turbine Engine Jet Noise and Plume IR Signature Attenuation," STTR Final Report (2009).
[9] Jordan, Peter, and Colonius, Tim, "Wave Packets and Turbulent Jet Noise," Annu. Rev. Fluid Mech. 2013.45:173-195.
[10] Ishii, Tatsuya, Tanaka, Nozomi, Oishi, Tsutomu, and Ishii, Yutaka, "Noise Test of Revised Notch Nozzle Using a Jet Engine," Brüel and Kjær Technical Review No. 1-2013, ed. Harry K. Zaveri (2013).

[11] Harley, Jacob L., Rolling, August J., Wisniewski, Charles F., and Gross, Kevin C., "Spatially resolved infrared spectra of F109 turbofan exhaust," AFIT (2012).
[12] Naval Research Advisory Committee, "Report on Jet Engine Noise Reduction," URL: http://www.nrac.navy.mil/docs/2009_FINAL_Jet_Noise_Report_4-26-09.pdf (2009).
[13] Fisher, M. J., Harper-Bourne, M., and Glegg, S. A. L., "Jet Engine Noise Source Location: The Polar Correlation Technique," Journal of Sound and Vibration 51:1, 23-54 (1977).
[14] http://www.spectralcalc.com/blackbody_calculator/blackbody.php
[15] Freund, Jonathan. "Jet Crackle." Technical Report AFRL-OSR-VA-TR-2015-0138, University of Illinois Urbana-Champaign 23 June 2015.
[16] Tam, Christopher K. W., Viswanathan, K., Ahuja, K. K., and Panda, J. "The sources of jet noise: experimental evidence." *J. Fluid Mech.* (2008), vol. 615, pp. 253-292.